Research Square

Preprints are preliminary reports that have not undergone peer review. They should not be considered conclusive, used to inform clinical practice, or referenced by the media as validated information.

Infrapatellar Fat Pad-derived Mesenchymal Stem Cell-based Spheroids Enhance Their Therapeutic Efficacy to Reverse Synovitis and Fat Pad Fibrosis

Dimitrios Kouroupis
University of Miami Miller School of Medicine: University of Miami School of Medicine
https://orcid.org/0000-0002-3892-9013
Melissa A Willman
University of Miami Miller School of Medicine: University of Miami School of Medicine
Thomas M Best
University of Miami Miller School of Medicine: University of Miami School of Medicine
Lee D Kaplan
University of Miami Miller School of Medicine: University of Miami School of Medicine
Diego Correa (dxc821@med.miami.edu)
Department of Orthopedics, UHealth Sports Medicine Institute, University of Miami, Miller School of Medicine, Miami, FL https://orcid.org/0000-0002-9004-4300

Research

Keywords: Mesenchymal Stem Cells (MSC), infrapatellar fat pad (IFP), CD146 subpopulations, cell priming, spheroid cultures, synovitis, IFP fibrosis, osteoarthritis

Posted Date: October 21st, 2020

DOI: https://doi.org/10.21203/rs.3.rs-94156/v1

License: This work is licensed under a Creative Commons Attribution 4.0 International License.
Read Full License

Version of Record: A version of this preprint was published on January 7th, 2021. See the published version at https://doi.org/10.1186/s13287-020-02107-6.

Infrapatellar fat pad-derived Mesenchymal Stem Cell-based spheroids enhance their therapeutic efficacy to reverse synovitis and fat pad fibrosis

Dimitrios Kouroupis,[1,2] Melissa A Willman,[2] Thomas M Best,[1] Lee D Kaplan,[1] and Diego Correa[1,2,*]

[1] Department of Orthopedics, UHealth Sports Medicine Institute, University of Miami, Miller School of Medicine, Miami, FL

[2] Diabetes Research Institute & Cell Transplantation Center, University of Miami, Miller School of Medicine, Miami, FL

CONTRIBUTIONS

All authors have made substantial contributions to the conception and design of the study, to obtaining and analyzing the data, to the drafting the article or revising it critically and to the final approval of the version to be submitted.

*** Corresponding author:**

Diego Correa, MD, MSc, PhD

Department of Orthopedics, UHealth Sports Medicine Institute; Diabetes Research Institute & Cell Transplant Center, University of Miami, Miller School of Medicine, 1450 NW 10th Ave (3014), Miami, FL, 33136 – USA

Phone: +1 (305) 243-2228; Fax: +1 (305) 243-4404; Email: dxc821@med.miami.edu

ABSTRACT

Background: To investigate the *in vitro* and *in vivo* anti-inflammatory/anti-fibrotic capacity of IFP-MSC manufactured as 3D spheroids. According to our hypothesis, IFP-MSC do not require prior cell priming to acquire a robust immunomodulatory phenotype *in vitro* in order to efficiently reverse synovitis and IFP fibrosis and secondarily delay articular cartilage damage *in vivo*.

Methods: Human IFP-MSC immunophenotype, tri-potentiality, and transcriptional profiles were assessed in 3D settings. Multiplex secretomes were assessed in IFP-MSC spheroids [Crude (non-immunoselected), $CD146^+$ or $CD146^-$ immunoselected cells] and compared with 2D cultures with and without prior inflammatory/fibrotic cell priming. Functionally, immunopotency limiting human PBMCs proliferation and effect on stimulated synoviocytes with inflammation and fibrotic cues. Finally, spheroids were tested *in vivo* in a rat model of acute synovitis/fat pad fibrosis.

Results: Spheroids enhanced IFP-MSC phenotypic, transcriptional and secretory immunomodulatory profiles compared to 2D cultures. Further, $CD146^+$ IFP-MSC spheroids showed enhanced secretory and transcriptional profiles, however, not reflected in a superior capacity to suppress activated PBMC suggesting 3D environment sufficient to induce an immunomodulatory phenotype. Crude IFP-MSC spheroids modulated the molecular response of synoviocytes previously exposed to inflammatory cues. Therapeutically, IFP-MSC spheroids retained Substance P degradation potential *in vivo*, while effectively induced resolution of inflammation/fibrosis of synovium and fat pad, halting the articular cartilage degradation in a rat model of progressive synovitis, fat pad fibrosis and osteoarthritis.

Conclusions: 3D spheroids confer IFP-MSC a reproducible and enhanced immunomodulatory effect *in vitro* and *in vivo*, circumventing the requirement of non-compliant cell priming or selection before administration, thus streamlining cell products manufacturing protocols.

Keywords: Mesenchymal Stem Cells (MSC); infrapatellar fat pad (IFP); CD146 subpopulations; cell priming; spheroid cultures; synovitis; IFP fibrosis; osteoarthritis

SIGNIFICANCE STATEMENT

The current comprehensive interrogation improves our understanding of Infrapatellar-fat pad mesenchymal stem cells (IFP-MSC) responses to osteoarthritis (OA) inflammation/fibrosis environment and whether those intrinsic responses can be induced following MSC purification and 3D spheroid culturing. This study, demonstrates that IFP-MSC spheroids possess enhanced anti-inflammatory/anti-fibrotic functional cell signature, circumventing the use of cell priming and streamlining manufacturing protocols. The resulting evidence

could be harnessed for the design of novel and/or to modify existing OA clinical protocols with IFP-MSC, with potentially more reproducible clinical outcomes.

BACKGROUND

Synovium and infrapatellar fat pad (IFP) tissues have been considered a single anatomical unit [1], actively participating in the modulation of the knee's intra-capsular homeostasis [2]. As such, this unit serves as a site of immune cell infiltration and active source of multiple pro-inflammatory/pro-fibrotic and articular cartilage catabolic mediators including tumor necrosis factor-alpha (TNF-α), interferon-gamma (IFN-γ), connective tissue growth factor (CTGF) and matrix metalloproteinases (MMPs) [3-9]. The associated synovium and IFP inflammation and fibrosis are intimately involved in the onset and progression of joint disease including Osteoarthritis (OA) [10-15]. Accordingly, targeting those local events could have a potential impact on altering the course of this chronic disease [16].

Facing the lack of disease-modifying therapeutic strategies in OA [17], novel alternatives are currently under clinical investigation including cell-based therapy approaches with encouraging initial results. For instance, early-stage clinical trials using either heterogeneous adipose-derived stromal vascular fraction cells [18], or expanded Mesenchymal Stem/Stromal Cells (MSC) derived from either umbilical cord [19] or bone marrow [20] have demonstrated clinical superiority when compared with current alternatives. Mechanistically, once reaching an inflammatory environment, MSC exert 'medicinal signaling' activities [21] due to their sensory capacity and secretion of immunomodulatory mediators such as the tryptophan depleting enzyme indoleamine 2,3Dioxygenase (IDO), interleukin-10 (IL-10), prostaglandin E2 (PGE2) and others [22,23], thereby resulting in strong anti-inflammatory effects. However, multiple clinical trials still show only moderate or even inconsistent results. To help circumventing this limitation, preclinical studies have shown that MSC can be "functionalized" *in vitro* (add ref 34) to enhance their therapeutic capacities, while simultaneously reducing the intrinsic phenotypic and functional variabilities within cell preparations.

MSC can be extracted from multiple sources including the knee's synovium and IFP [24,25]. IFP-MSC constitute a promising alternative for the treatment of OA and other joint disorders given their presence within the joint environment, ease of harvest during knee arthroscopy, and high proliferation rate *in vitro* [24,26]. To that end, we have shown that IFP-MSC possess an intrinsic immunomodulatory secretory profile, involving *in vitro* and *in vivo* efficient degradation of the nociception and inflammation regulator Substance P (SP) through a CD10 (neprilysin/NEP)-dependent manner, resulting in synovial and IFP inflammation and fibrosis reversal. Importantly, these specific attributes and functions can be induced or further enhanced *in vitro* prior to the administration of the cells. On this basis, we have reported that IFP-MSC exposed to inflammatory cues including TNF-α, IFN-γ, and CTGF (*i.e.,* cell priming/licensing) and/or expanded under regulatory-compliant conditions

(*e.g.,* pooled human platelet lysate - hPL) can effectively reinforce the critical $CD10^+$ phenotype, which translates into enhanced functional properties both *in vitro* and *in vivo* [27-29].

On the other hand, we have also recently reported that a similar inflammatory cell priming protocol applied to bone marrow-derived MSC (BM-MSC) enriches the preparation in $CD146^+$ cells, unveiling a subset with innately higher immunomodulatory and secretory capacities compared to their $CD146^-$ counterparts [30]. A comparable CD146-dependent phenotypic and functional discrimination in IFP-MSC has not been reported yet. Consequently, coupling CD146 with CD10-dependent phenotype-based MSC purification of heterogeneous preparations could result in cell products with combined enhanced biological functions, as previously shown for other defining markers such as CD271 [31,32].

MSC possess a remarkable ability to coalesce and assemble in tri-dimensional (3D) structures (*i.e.*, MSC spheroids) that closely recapitulate the *in vivo* MSC niche by providing spatial cell organization with increased cell-cell interactions. In that context, 3D spheroids provide MSC a stable immunophenotypic profile, with reinforced survival, homing, stemness, differentiation potential, angiogenic and anti-inflammatory properties [33]. MSC-based spheroids have been applied in various preclinical models including wound healing, bone and osteochondral defects and cardiovascular diseases showing safety and efficacy (reviewed in [34]).

Based on this collective information, the current study explores the effects on the phenotypic, transcriptional, secretory and functional profiles of an IFP-MSC cell-based product when manufactured as 3D spheroids and following phenotype-based MSC purification, expanding our understanding of IFP-MSC responses to inflammatory/fibrotic environments. The resulting evidence could be harnessed to serve as a foundation for the design of novel and/or to modify existing clinical protocols with IFP-MSC for joint disease including OA based on cell therapy, with potentially more reproducible clinical outcomes.

METHODS

Cell and animal protocols

IFP-MSC were isolated from IFP tissue obtained from de-identified, non-arthritic patients (seven males and six female, with an age range between 17-60 years-old) undergoing elective knee arthroscopy at the Lennar Foundation Medical Center - University of Miami and after provided written informed consent. All procedures were carried out in accordance with relevant guidelines and regulations and following a protocol determined by the University of Miami IRB not as human research (based on the nature of the samples as discarded tissue). IFP tissue (<20ml) was mechanically dissected and washed repeatedly with Dulbecco's Phosphate Buffered Saline (PBS; Sigma), followed by enzymatic digestion using 235 U/ml Collagenase I (Worthington Industries, Columbus, OH) diluted in PBS and 1% bovine serum albumin (Sigma) for 2 hours at 37^{o}C with agitation. Cell digests were inactivated with complete media [DMEM low glucose GlutaMAX (ThermoFisher Scientific,

Waltham, MA) +10% fetal bovine serum (FBS; VWR, Radnor, PA], washed and seeded at a density of $1x10^6$ cells/175 cm^2 flask in complete media.

The animal protocol was approved by the Institutional Animal Care and Use Committee (IACUC) of the University of Miami, USA (approval no. 16-008-ad03) and conducted in accordance to the ARRIVE guidelines (Kilkenny et al., 2012). Sixteen (#16) 10-week old Sprague Dawley rats (8 males and 8 females; mean weight 250 g and 200 g, respectively) were used. The animals were housed to acclimate for 1 week before the experiment initiation. One rat was housed per cage in a sanitary, ventilated room with controlled temperature, humidity, and under a 12/12 hour light/dark cycle with food and water provided ad libitum.

Culture of IFP-MSC and synoviocytes

IFP-MSC were cultured at 37°C 5% (v/v) CO_2 until 80% confluent (denoted as P0), then passaged at a 1:5 ratio until P3 detaching them with TrypLE™ Select Enzyme 1X (Gibco, ThermoFisher Scientific) and assessing cell viability with 0.4% (w/v) Trypan Blue (Invitrogen, Carlsbad, CA). Synoviocytes (Sciencell, Carlsbad, USA) were cultured using synoviocyte medium (Sciencell) at 37°C 5% (v/v) CO_2 until 80% confluent (denoted as P0), then passaged at a 1:4 ratio until P2 detaching them with TrypLE™ Select Enzyme 1X (Gibco, ThermoFisher Scientific) and assessing cell viability with 0.4% (w/v) Trypan Blue (Invitrogen, Carlsbad, CA).

IFP-MSC spheroids were created using gas-permeable culture plates (Miltenyi Biotech, Inc., Auburn, CA). Briefly, $2x10^5$ cells resuspended in DMEM/10%FBS + Methylcellulose solution (4/1 ratio) were seeded per well of a 6-well gas-permeable culture plate and cultured for 2 days at 37°C and 5% CO_2. MSC spheroids were evaluated for phenotypic, secretory, transcriptional, and functional profiles. Graphical abstract shows the experimental set-up of the study.

CD146 surface marker-based magnetic immunoselection

Immunomagnetic cell sorting was performed in P1 Crude IFP-MSC (n=5). Briefly, 2×10^6 cells Crude IFP-MSC were resuspended in 1X PBS with 0.5% bovine serum albumin (BSA) and 2 mM EDTA and incubated with biotinylated anti-human CD146 (Miltenyi Biotech) at 4˚C for 20 minutes with agitation. Invitrogen™ CELLection Dynabeads™ Biotin Binder Kit (Thermo Fisher Scientific) was used for magnetic immunoselection resulting in the CD146POS and CD146NEG subpopulations according to manufacturer's instructions. The generated P2 CD146POS and P2 CD146NEG subpopulations were directly plated and expanded with DMEM/10%FBS until 70-80% confluency. All IFP-MSC subpopulations were stored in liquid nitrogen until further experimentation.

Immunophenotype

IFP-MSC spheroids reverse synovitis/IFP fibrosis

Flow cytometric analysis was performed on P3 naïve IFP (n=3) MSC. 2.0 x 10^5 cells were labelled with fluorochrome-conjugated monoclonal antibodies specific for: CD10, CD44, CD56, CD90 (Biolegend, San Diego, CA), CD146 (Miltenyi Biotech), NG2 (BD Biosciences, San Jose, CA), CXCR4 (Invitrogen) and the corresponding isotype controls. Immunophenotyping marker selection was based on our previous data which associate their expression levels with distinct immunomodulatory signatures and functionalities. All samples included a Ghost Red Viability Dye (Tonbo Biosciences, San Diego, CA). Data were acquired using a Cytoflex S (Beckman Coulter, Brea, CA) and analysed using Kaluza analysis software (Beckman Coulter).

Immunofluorescence was performed on P3 IFP-MSC spheroids (n=3) in suspension cultures. Briefly, IFP-MSC spheroids were fixed in 3.7% paraformaldehyde for 1 hour at RT, permeabilized with 0.2% Triton-X/gelatin solution for 1 hour, and subsequently with 0.5% Triton-X/gelatin solution for 15 minutes. Fixed/permeabilized IFP-MSC spheroids were incubated with unconjugated primary antibodies CD10, CD44, CD90 (Abcam, Cambridge, MA), CD146 (Miltenyi Biotech), CXCR4 (Abcam), NG2 (Invitrogen) overnight at 4°C. Next day, the spheroids were washed 5x with 0.2% Triton-X and incubated with secondary antibodies for 1 hour. After rinsing 5x with 0.2% Triton-X and incubation with DAPI (Invitrogen) for 10 minutes, images were captured on a Leica TCS SP5 confocal microscope using 20x objective and evaluated with ImageJ software. All quantifications were performed in at least 5 regions of interest (ROIs) per IFP-MSC spheroid and in total 5 spheroids per IFP-MSC spheroid subpopulation. Quantitations were performed using the formula: corrected total cell fluorescence (CTGF)= integrated density – (area of selected cell X mean fluorescence of background readings).

Quantitative real-time PCR (qPCR)

RNA extraction was performed using the RNeasy Mini Kit (Qiagen, Frederick, MD) according to manufacturer's instructions. Total RNA (1µg) was used for reverse transcription with SuperScript™ VILO™ cDNA synthesis kit (Invitrogen), and 10 ng of the resulting cDNA was analysed by qPCR using QuantiFast SYBR Green qPCR kit (Qiagen) and a StepOne Real-time thermocycler (Applied Biosystems, Foster City, CA). For each target, human transcript primers were selected using PrimerQuest (Integrated DNA Technologies, San Jose, CA) (Supplementary Table S1). All samples were analysed in triplicate. Mean values were normalized to GAPDH, expression levels were calculated using the $2^{-\Delta\Delta}$Ct method and represented as the relative fold change of the primed cohort to the naïve (=1).

A pre-designed 90 gene Taqman-based mesenchymal stem cell qPCR array (Stem Cell Technologies, Supplementary Table S2) was performed (n=3) using 1000 ng cDNA per IFP-MSC sample and processed using StepOne Real-time thermocycler (Applied Biosystems). Data analysis was performed using Stem Cell technologies qPCR online analysis tool (Stem Cell Technologies). Sample and Control Ct Values were expressed as 2^-ΔCt (with 38 cycles cut-off point). The expression levels were represented in bar plots ranked by transcript

expression levels on a log-transformed scale of sample compared to control cohorts. Bar plots were colour-coded by the functional class of genes (namely Stemness, MSC, MSC-related/Angiogenic, Chondrogenic/Osteogenic, Chondrogenic, Osteogenic, Adipogenic). A t-test (unpaired, two-tailed test with equal variance) is used in all statistical analysis and p-values were corrected for multiple comparisons by the Benjamini-Hochberg procedure. Two groups were compared and presented in bar plots: sample (spheroids) versus control (2-D cultures), and sample (CD146POS spheroids) versus control (Crude spheroids).

Trilineage differentiation

Osteogenic, chondrogenic and adipogenic differentiation potential was evaluated in P3 IFP-MSC spheroids (n=3) similar to previously published protocols [35]. Briefly, MSC spheroids were created using gas-permeable culture plates (Miltenyi Biotech) and methylcellulose and cultured for 2 days at 37°C and 5% CO_2 as described above. On day 2, IFP-MSC spheroids were subsequently induced towards osteogenesis, adipogenesis, and chondrogenesis by changing the medium to induction media in the separate gas-permeable culture plate wells. Differentiation status of 3-D IFP-MSC spheroids was evaluated by the expression levels of specific differentiation-related transcripts using qPCR (Supplementary Table S1).

Secretome analysis

Arrays for growth factors (GFs) and inflammatory mediators (RayBio® C-Series, RayBiotech, Peachtree Corners, GA) were used to determine secreted levels obtained from Crude 2-D IFP-MSC, and Crude and CD146-selected IFP-MSC spheroids pre- and post-priming. For each population, 1 mL of conditioned media obtained from 2 donors, was prepared and used for each assay following the manufacturer's instructions. Data shown represent 40 sec exposure in FluorChem E chemiluminescence imaging system (ProteinSimple, San Jose, CA). Results were generated by quantifying the mean spot pixel density of each array using protein array analyser plugin using ImageJ software (Fiji/ImageJ, NIH website). The signal intensities were normalized with the background whereas separate signal intensity results represent the average pixel density of two spots per protein. The signal intensity for each protein spot is proportional to the relative concentration of the antigen in the sample.

Pathway analysis

Putative interactomes were generated by Search Tool for Retrieval of Interacting Genes/Proteins (STRING 11.0; available from: http://string-db.org) [80] database using interaction data from experiments, databases, neighbourhood in genome, gene fusions, co-occurrence across genomes, co-expression and text-mining. An interaction confidence score of 0.4 was imposed to ensure high interaction probability. K-means

clustering algorithm was used to organize proteins into 3 separate clusters per condition tested, discriminated by colours. Venn diagrams were used to demonstrate all possible relations between Crude and CD146-selected IFP-MSC subpopulations post-TI and -TIC priming for the significantly ($p<0.05$) altered proteins. Functional enrichments related to biological process, Kyoto Encyclopedia of Genes and Genomes (KEGG) pathways, and reactome pathways were presented in radar graphs for all conditions tested. Seven biological processes were evaluated namely positive regulation of cell population proliferation (GO:0008284), positive regulation of response to stimulus (GO:0048584), positive regulation of cell migration (GO:0030335), regulation of signal transduction (GO:0009966), regulation of signaling receptor activity (GO:0010469), positive regulation of protein phosphorylation (GO:0001934), and angiogenesis (GO:0001525). Additionally, eight KEGG reactome pathways were evaluated including cytokine-cytokine receptor interaction (hsa:04060), MAPK signaling (hsa:04010), PI3K-Akt signaling (hsa:04151), Ras signaling (hsa:04014), Jak-STAT signaling (has:04630), Rap1 signaling (has:04015), signaling by interleukins (HSA: 449147), and interleukin-10 signaling (HSA: 6783783).

Indoleamine 2,3-Dioxygenase (IDO) *in vitro* assay

IDO SimpleStep ELISA kit (Abcam, MA, USA) was used to quantify the secreted levels (pg/ml) Crude and CD146-selected IFP-MSC spheroids with and without priming (10^5 IFP-MSC/well, 12-well; n=3 per cohort), following manufacturer's instructions. IDO secretion was quantified in centrifuged (1500 rpm; 5 minutes) conditioned media (run in duplicates within the membrane) obtained from IFP-MSC cultures in all conditions. Levels were determined by measuring the fluorescence (450nm) of individual wells in end-point mode (SpectraMax M5 spectrophotometer, Molecular Devices, San Jose, CA, USA). IDO secretion was normalized to total protein secreted per cohort.

Prostaglandin E_2 *in vitro* assay

Parameter Prostaglandin E_2 (PGE_2) competitive immunoassay (R&D Systems, MN, USA) was used to quantify the secreted levels (pg/ml) in Crude and CD146-selected IFP-MSC spheroids with and without priming (10^5 IFP-MSC/well, 12-well; n=3 per cohort), following manufacturer's instructions. PGE_2 was quantified in conditioned media (run in duplicates within the membrane) obtained from IFP-MSC cultures in all conditions. Levels were determined by subtracting measured optical densities of individual wells at 450nm and 540nm in end-point mode (SpectraMax M5 spectrophotometer, Molecular Devices), and converted into concentrations using the reference standard curve run with the assay. IDO secretion was normalized to total protein secreted per cohort.

Immunopotency assay (IPA)

IFP-MSC spheroids reverse synovitis/IFP fibrosis

Crude and CD146-selected IFP-MSC spheroids (n=3) were designated into non-induced or TIC-primed cohorts. After 72 hours in complete culture (non-induced) or TIC priming (primed) media, IFP-MSC cultures were washed once with PBS and media were changed to IPA medium containing RPMI (Gibco) with 15% Human AB Serum (Corning, Corning, NY, USA), 1% L-glutamine (Gibco), 1% Non-Essential Amino Acids (Gibco), 1% Sodium Pyruvate, 1% HEPES (Gibco), and 1% 100X Vitamins (Gibco). Human peripheral blood mononuclear cells (PBMC) (Continental Services Group Blood Bank, Miami, USA) were stained with CellTrace^{TM} CFSE Cell Proliferation Kit (Invitrogen) according to manufacturer's instructions and resuspended in IPA media. PBMC/IFP-MSC non-contact co-cultures were performed by seeding CFSE-stained PBMCs in the lower chamber of a 12-well plate and non-induced or TIC-primed IFP-MSC spheroids in transwells (0.4μm pore size, Corning) in IPA medium at a 2:1 ratio. Cell stimulation cocktail 500x (Invitrogen) containing phorbol 12-myristate 13-acetate and ionomycin was then added to the wells designated for PBMC stimulation. After 96 hours, CFSE-stained cells were collected, stained with Ghost Red 780 Viability Dye (Tonbo Biosciences), and acquisition of 10,000 was performed using a CytoFLEX S cytometer with CytExpert software (Beckman Coulter). PBMCs were gated by scatter, viability, and CFSE positivity, and PBMC proliferation was represented as $CFSE^{dim}$/total CFSEx100.

MSC and synoviocyte priming

Crude P3 IFP-MSC (n=5) were seeded in 2D or 3D settings in 6-well plates at a density of $2x10^5$ cells/well in complete medium. Next day (24 hours), cultures were primed with TI inflammatory cocktail (15 ng/ml TNFα, 10 ng/ml IFNγ) for 48 hours or TIC inflammatory/fibrotic cocktail (15 ng/ml TNFα, 10 ng/ml IFNγ, 10 ng/ml CTGF) for 72 hours. Non-induced and both TI- and TIC- primed cohorts were evaluated for secretory and transcriptional profiles. Non-induced and TIC-primed cohorts were evaluated for functional profiles.

IFP-MSC/Synoviocyte co-cultures

P3 synoviocytes were seeded in 6-well plates at a density of $2x10^5$ cells/well in synoviocyte medium. Next day (24 hours), synoviocyte cultures were designated into non-induced or TIC-primed cohorts and cultured for 3 days with the appropriate medium. On day 3, synoviocyte/IFP-MSC co-cultures were performed by seeding non-induced IFP-MSC spheroids on top of synoviocyte monolayers at a density of $5x10^5$ cells/well. Co-cultures were fed with synoviocyte medium or synoviocyte medium + TIC inflammatory/fibrotic cocktail (15 ng/ml TNFα, 10 ng/ml IFNγ, 10 ng/ml CTGF) for 72 hours according to the initial non-induced or TIC-primed cohorts designation. Non-induced and primed cohorts were evaluated for secretory and transcriptional profiles. Microscope images of IFP-MSC/Synoviocyte co-cultures were acquired using 10x objective Leica DMi8 microscope with Leica X software (Leica).

Mono-iodoacetate model of acute synovial/IFP inflammation

Acute synovial/IFP inflammation was generated by intra-articular injection of 1 mg of mono-iodoacetate (MIA) in 50 µl of saline in the right knee. Briefly, under isoflurane inhalation anesthesia rat knees were flexed 90º and MIA was injected into the medial side of the joint with a 27G needle using the patellar ligament and articular line as anatomical references. This short exposure to MIA has been shown to induce inflammatory changes at the synovium and adjacent IFP [36]. Three (3) days later, a single intra-articular injection of 500,000 IFP-MSC spheroids in 50 µl of Euro-Collins solution (MediaTech) was performed (similar injection technique), having as control: 1) rats receiving MIA but not IFP-MSC (Only MIA group); and 2) healthy rats receiving only IFP-MSC spheroids (Only IFP-MSC group). Animals were sacrificed at two different timepoints: 4 and 25 days after IFP-MSC injection (day 7 and day 28 total, respectively).

Tissue preparation and histological analysis

Rat knee joints were harvested by cutting the femur and tibia/fibula 1 cm above and below the joint line, muscles were removed and joints were fixed with 10% neutral buffered formalin (Sigma-Aldrich) for 14 days at room temperature. Knee joints were decalcified, cut at sagittal plane in half, embedded in paraffin and serial 4 µm sections were obtained. Hematoxylin and Eosin (H&E) staining was performed to evaluate the structure and morphology of knee joints. Masson's Trichrome staining for collagen-rich fibrotic areas was used to evaluate the extent of fibrosis in fat pad tissue. Toluidine blue staining for cartilage proteoglycan subunits was used to evaluate articular cartilage quality changes. Microscope images of cytochemically stained tissues were acquired using 10x and 20x objectives Leica DMi8 microscope with Leica X software (Leica). Based on histochemical stainings, tissue synovitis/fibrosis was evaluated in 3 rat knees per condition and 4 microscopy fields per knee with ImageJ software.

For anti-substance P immunofluorescence staining, sections were incubated with 1x citrate buffer solution at 60 °C overnight for antigen retrieval, permeabilised with 1x PBS + 0.2% Triton X-100 for 20 minutes at room temperature, and incubated with blocking buffer (1x PBS + 0.1% Triton X-100 with 10% rabbit serum) for 1 hour at room temperature. In between different treatments sections were washed with 1x PBS. Rabbit anti-rat substance P polyclonal antibody (Millipore) was prepared in blocking buffer (1:100) and sections were incubated at 4 °C overnight. Sections were washed with 1x PBS + 0.01% Triton X-100 and incubated for 1 hour with secondary antibody containing Alexa Fluor594 conjugated goat anti-rabbit IgG antibody (Thermo Fisher Scientific) at room temperature. Controls were incubated with secondary antibody only. All sections were rinsed with 1x PBS, mounted in prolong gold antifade reagent with DAPI (Invitrogen), and microscope images were acquired using 10x objective Leica DMi8 microscope with Leica X software (Leica). Substance P tissue distribution was evaluated in 3 rat knees per condition and 4 microscopy fields per knee with ImageJ software.

Statistical analysis

Statistical analysis was performed using paired and unpaired Student's *t*-test for normally distributed data and Wilcoxon (for paired data) or Mann Whitney (for unpaired data) test in presence of a non-normal distribution; one-way ANOVA was used for multiple comparisons. All tests were performed with GraphPad Prism v7.03 (GraphPad Software, San Diego, CA). Level of significance was set at $p < 0.05$. Data used for the statistical analyses is indicated in the figure legends, overall corresponding to three independent experiments from different MSC donors (n=3), unless specified.

RESULTS

Phenotypic characterization of 2D IFP-MSC and IFP-MSC spheroids

A complete immunophenotyping of IFP-MSC expanded in DMEM/10%FBS and other regulatory-complaint formulations have been previously reported in [27-29]. Herein, we confirm the stable MSC-related phenotypic profile of IFP-MSC expanded in 2D cultures (Figure 1A).

Crude IFP-MSC seeding with methylcellulose in gas-permeable culture plates for 2 days result in the generation of multiple sized (100-300μm) non-adherent IFP-MSC spheroids which show compact spheroid intra-structural organization with increased cell-cell interactions and no necrotic core, implying the physiological nutrient and gas supply reaching the center of every individual spheroid (Figure 1B). Immunophenotypic profiling of the generated spheroids revealed enhanced and similar between different spheroids expression of CD90 (308±15 AU), CXCR4 (226±14 AU), CD10 (192±45 AU), and NG2 (331±83 AU). Interestingly, CD146 show high expression levels but variable between different spheroids (245±141 AU) whereas CD44 showed also high variability (371±179 AU) (Figure 1C).

In order to evaluate the differentiation capacity of generated IFP-MSC spheroids we have performed tripotentiality assessment *in vitro* showing that upon specific induction in gas-permeable plates IFP-MSC spheroids can efficiently differentiate towards chondrogenic, osteogenic and adipogenic lineages (Figure 1D). Quantitatively at the molecular level, crude IFP-MSC spheroids show significantly ($p<0.05$) higher expression levels for chondrogenic genes *ACAN* and *COMP*, the osteogenic gene *OMD,* adipogenic genes *FABP4* and *PPARγ* compared to non-induced controls, indicating their increased maturity during the different differentiation schemes.

Molecular and secretory profiles comparison of 2D IFP-MSC and IFP-MSC spheroids

Molecular profiling of IFP-MSC spheroids versus 2D IFP-MSC cultures revealed that 49 out of 90 genes tested were higher expressed in IFP-MSC spheroids with 24 genes being more than two-fold higher (*IBSP, COL10A1, BMP2, MMP13, LIF, IL10, IFNG, SP7, ITGAX, SOX2, COL2A1, BMP7, PROM1, FGF10, NES, IL6, TGFB3, TERT, BMP6, RUNX2, GDF15, TGFB1, FZD9, IGF1*). Interestingly, genes tested were grouped in

phenotype/function-related cohorts with stemness cohort showing overall the most prominent fold expression change between IFP-MSC spheroids and 2D IFP MSC cultures (Figure 2A).

The secretory profile of inflammation-related cytokines revealed that IFP-MSC spheroids show significantly ($p<0.05$) higher secretion of 13 and lower secretion of 5 (IL-6, IL-6sR, IL-16, MIP-1-β, TNF-α) out of 40 secreted proteins tested compared to 2D IFP-MSC cultures (Figure 2B). Among the highly secreted proteins in IFP-MSC spheroids were: IL-1α, IL-7, IL-8, IL-11, IL-12-p70, M-CSF, MIG, MIP-1-α, MIP-1-δ, sTNF-RI, sTNF-RII, PDGF-BB, and TIMP-2. Interestingly, spheroid culturing of IFP-MSC result in lower secretion of IL-6 and higher secretion of IL-8 protein, which associates with significantly lower IL-6/IL-8 ratio suggesting a less pro-inflammatory status compared to 2D IFP-MSC cultures. Upon TI-induction, IFP-MSC spheroids showed increased secretion of 11 (Eotaxin-2, G-CSF, GM-CSF, IFN-γ, I-309, IL-2, IL-11, MIP-1-α, RANTES, PDGF-BB, and TIMP-2) and decreased secretion of 6 (IL-6, IL-6sR, IP-10, MCP-1, MCP-2, TNF-α) proteins compared to 2D IFP-MSC cultures. Importantly, the overall protein secretion of inflammation-related cytokines in IFP-MSC spheroids is reduced compared to 2D IFP-MSC cultures in both non-induced and TI-induced conditions (1.1-fold and 1.2-fold, respectively Figure 2C).

In contrast, IFP-MSC spheroids strongly secrete reparative growth factors compared to 2D IFP-MSC cultures even without TI induction (Figure 2B). Specifically, IFP-MSC spheroids show significantly ($p<0.05$) higher secretion of 36 out of 41 secreted protein tested. Upon TI induction, the amount of significantly higher secreted proteins in IFP-MSC spheroids is reduced as 2D IFP-MSC cultures increase their overall secretory profile. Therefore, the overall IFP-MSC spheroid growth factor secretory profile is enhanced compared to 2D IFP-MSC cultures in both non-induced and TI-induced conditions (1.9-fold and 1.32-fold, respectively Figure 2C).

Crude and CD146-selected IFP-MSC spheroids show distinct phenotypic and molecular profiles

CD146-based magnetic immunoselection of crude IFP-MSC resulted in the generation of two separate subpopulations (CD146POS and CD146NEG) with distinct immunophenotypic profiles (Figure 3A). Specifically, CD146POS IFP-MSC spheroids show as expected higher expression levels of CD146 (451±4 AU vs 249±18 AU) and higher expression levels of NG2 (362±178 AU vs 287±22 AU) compared to CD146NEG IFP-MSC spheroids, indicating their enhanced pericytic phenotype (Figure 3A, left panel). Interestingly, CD146 expression is not absent in CD146NEG IFP-MSC spheroids suggesting that 3D spheroid culturing *in vitro* can positively affect CD146 expression levels (Supplementary Figure 1A). Importantly, this CD146 protein presence is coupled with gene expression, which shows not only its up-regulation in 3D settings but also significant expression also in the CD146NEG cohort (Figure 3B). In parallel, CD146NEG IFP-MSC spheroids show higher expression levels of CD10 (253±27 AU vs 164±13 AU) and CXCR4 (227±3 AU vs 140±14 AU) compared to CD146POS IFP-MSC spheroids (Figure 3A, right panel). Putatively, low expression levels of surface bound

IFP-MSC spheroids reverse synovitis/IFP fibrosis

CD10 in CD146POS IFP-MSC spheroids is correlated with high CD10 secretion capacity as we previously reported [27]. Interestingly, in CD146POS CD44 (682±62 AU vs 333±64 AU) and CD90 (429±83 AU vs 294±24 AU) had higher expression levels compared to CD146NEG IFP-MSC spheroids, possibly associated with their pericytic phenotype and increased stemness *in vitro*.

Molecular profiling of CD146POS versus CD146NEG IFP-MSC spheroids revealed that 55 out of 90 genes tested were higher expressed in CD146POS IFP-MSC spheroids with 12 genes being more than two-fold higher (*MCAM, HGF, ALPL, DLX5, NES, MMP13, CD200, COL1A1, FZD9, PDGFRB, HIC1*). Interestingly, genes tested were grouped in phenotype/function-related cohorts with chondrogenesis and MSC-related/angiogenesis cohorts showing overall the most prominent fold expression change between CD146POS and CD146NEG cohorts (Figure 3C). By comparing the significantly up-regulated genes in Crude spheroids versus 2D cultures (Figure 2A) and the significantly up-regulated genes in CD146POS versus CD146NEG cohorts, 26 genes are shared between Crude and CD146POS spheroids, indicating similarities in their molecular signatures (Figure 3D). However, upon TI- or TIC- induction most of the immunomodulatory-related genes tested show up-regulated expression levels in CD146POS spheroids (Supplementary Figure 1B).

Crude and CD146-selected IFP-MSC spheroids exhibit a robust secretion of reparative growth factors with and without exposure to priming inflammatory/fibrotic cues

Crude and CD146-selected IFP-MSC spheroids show similar inflammation-related secretory profiles both in non-induced and TI- or TIC-induced conditions. However, their secretory profiles of reparative growth factors were distinct and characterized by the secretion of different numbers and types of proteins (Figure 4A & 4B). Specifically, in non-induced conditions, when comparing the CD146POS with Crude IFP-MSC spheroids 6 proteins show significantly higher (FGF-6, EGF R, IGFBP-4, IGFBP-6, IGF-I sR, and IL-6 sR, $p<0.05$) and 5 proteins significantly lower (βFGF, IGFBP-1, SCF, PDGF-AB, and IL-4, $p<0.05$) secretion levels in CD146POS spheroids. Upon TI induction, CD146POS IFP-MSC spheroids show higher number of proteins with up-regulated (26) and lower number of proteins with down-regulated (1) secretion levels compared to other spheroid cohorts (Supplementary Figure 2A). Interestingly, among the proteins with up-regulated secretion levels after TI induction, 6 proteins were commonly shared between the three different cohorts (Figure 4C). A similar pattern was observed in all three different cohorts after TIC induction with CD146POS IFP-MSC spheroids, having up-regulated secretion of 24 proteins and down-regulated secretion of only 1 protein (Supplementary Figure 2B). However, among the proteins with up-regulated secretion levels after TIC induction, none are shared among the three different cohorts (Crude, CD146POS, CD146NEG), putatively indicating further secretory profile distinction between cohorts (Figure 4C).

In TI-induced IFP-MSC spheroids all subpopulation cohorts revealed overall similar biological processes involvement (Supplementary Figure 3A). In TIC-induced IFP-MSC spheroids, Crude cohort showed higher

involvement in 4 out of 7 biological processes tested (Supplementary Figure 3B). Overall, in both TI- and TIC-induced IFP-MSC spheroids, CD146POS cohort showed significantly stronger protein involvement in 4 out of 8 KEGG reactome pathways (MAPK, PI3K-Akt, Ras, and Rap1 signaling pathways) compared to other cohorts.

In non-induced cohorts IDO secretion was almost absent whereas TIC-induced IFP-MSC spheroids showed significantly (p<0.05) higher IDO secretion (80-fold for Crude, 73-fold for CD146POS, and 89-fold for CD146NEG; Figure 4D). Importantly, PGE2 secretion was evident in all non-induced cohorts with CD146POS spheroids showing significantly (p<0.05) higher secretion levels (in average 151pg/ml compared to 34.7 and 46.1pg/ml for Crude and CD146NEG, respectively). As expected, upon TIC induction PGE2 secretion was similarly increased in all three different cohorts but CD146POS had a higher trend of PGE2 secretion compared to others (Figure 4D).

Crude and CD146-selected IFP-MSC spheroids show enhanced immunomodulatory function *in vitro*

CFSE-labeled, PMA/IO-activated human PBMC showed a proliferation of ~91.2% for male PBMC donors and of ~89.9% for female PBMC donors, which was suppressed in a PBMC gender-dependent manner by non-contact co-culture with non-induced Crude or CD146-selected IFP-MSC spheroids (Figure 5A). On this basis, slightly enhanced PBMC suppression was observed when IFP-MSC spheroids were co-cultured with female PBMC donors. All non-induced Crude, CD146POS, and CD146NEG IFP-MSC cohorts show similar suppression capacity of the activated PBMC proliferation, ranging between 19.5 to 20.5% for male PBMC and 24.1 to 24.6% for female PBMC donors. Importantly, TIC induction of Crude or CD146-selected cohorts did not result in enhanced suppression capacity over activated PBMC.

Effects of IFP-MSC on synoviocytes response to inflammation *in vitro*

To assess the capacity of IFP-MSC spheroids to attach to synoviocyte monolayer *in vitro* and exert immunomodulatory effects, SYN/IFP-MSC spheroid co-cultures have been performed. In both non-induced and TIC-induced SYN, Crude IFP-MSC spheroids can effectively attach and form explant-cultures by expanding on a synoviocytes monolayer (Figure 5B). Importantly, TIC induction of SYN significantly (p<0.05) up-regulated inflammatory genes such as CD13 and PD-1 even at the presence of IFP-MSC spheroids in culture. However, SYN/IFP-MSC spheroid co-cultures resulted in significantly (p<0.05) higher secretion of 6 immunomodulatory proteins compared to TIC-induced SYN alone. Of note, SYN/IFP-MSC spheroid co-cultures result in significantly lower IL-6/IL-8 ratio from TIC-induced SYN alone, indicating the reduced inflammatory environment of such *in vitro* co-culture (Figure 5C).

IFP-MSC spheroids strongly reverse synovitis and IFP fibrosis and degrade SP *in vivo*

IFP-MSC spheroids reverse synovitis/IFP fibrosis

A rat model of induced acute synovitis and IFP fibrosis was used to test the capacity of IFP-MSC spheroids to reverse synovium and IFP inflammation and fibrosis (Figure 6). Compared to healthy rat knees, MIA group showed not only strong synovitis and fibrosis of the IFP tissue but also hyperinnervation by SP-positive sensory fibers 7 days after the intra-articular injection of MIA. Previously, we clearly demonstrated the transient engraftment of injected single cell IFP-MSC in areas of active synovitis and IFP fibrosis [27]. Herein, four days after IFP-MSC spheroid injection we observed significant reduction of synovitis and IFP fibrosis (from 45±2.5% to 24.5±4.3%) that was further reversed up to day 28 (17±3.5%). According to Udo et al. infrapatellar fat pad inflammation scoring (0-5) for rat arthritis induced by MIA [36], only MIA (untreated) cohort developed grade 3 synovitis and grade 2 to 3 fibrosis at the main IFP body, which were independent from rat gender. In addition, SP presence was significantly diminished (1.75-fold on day 4 and 5.9-fold on day 25) after IFP-MSC injection in both peripheral areas of the IFP (close to the synovium) and inner parts (IFP body) (Figure 6B). After 28 days of MIA injection, all animals developed articular cartilage structural changes compatible with OA lesions, mostly associated with reduction of the matrix staining and integrity. IFP-MSC spheroid injection showed articular cartilage with preserved matrix, evident by the strong toluidine blue staining of the structural sGAG. Quantification according to Udo et al. macroscopic scoring (0-5) for rat arthritis induced by MIA [36], only MIA (untreated) cohort developed grade 3 erosion (≤50% of joint surface) whereas IFP-MSC spheroid cohort showed almost intact articular surface (grade 0), which were independent from rat gender.

DISCUSSION

We have previously underlined the importance of *ex vivo* MSC "functionalization" for improved therapeutics *in vivo* [34]. Consequently, herein we investigated the cellular and molecular effects of spheroid culturing, CD146-based subset selection and response to inflammatory and fibrotic environments on IFP-MSC immunomodulatory and therapeutic properties in the context of synovitis/fibrosis reversal *in vivo*.

Importantly, our proposed gas-permeable cultures resulted in IFP-MSC spheroids without necrotic core, circumventing any oxygen and nutrients core exchange limitations associated with other spheroid culturing platforms [37]. Overall, we found that IFP-MSC spheroid culturing resulted in enhanced phenotypic, transcriptional and secretory profiles compared to 2D cultures. This includes enrichment for 'stemness' gene cohort as previously reported with other MSC types [38], increased CD146, CD10, NG2, and CXCR4 levels, higher tripotential differentiation capacity, and significantly enhanced reparative growth factor secretion (1.9-fold and 1.32-fold, respectively). Collectively, these data demonstrate the reinforcing effect of spheroid culturing on IFP-MSC propensities even in non-induced cultures without any exogenous pro-inflammatory/pro-fibrotic priming. Upon CD146-based selection, the generated subpopulations showed distinct protein, molecular and secretory profiles, similar to our previous report with BM-MSC [30]. As highlighted in our previous reports CD146 and CD10 are both key molecules correlated with increased immunomodulatory MSC functionality [27-

29]. However, solely 3D culturing settings had significant impact on IFP-MSC subpopulation phenotype as at the transcript level *CD146* gene expression was equally upregulated between the different cohorts (Crude, CD146POS, CD146NEG) compared to 2D cultures. This finding is of outmost importance indicating that MSC manufacturing in 3D settings can boost their immunomodulatory functionality without any further induction. Furthermore, both Crude and CD146POS cohorts share 26 highly upregulated genes that are mainly involved (13 out of 26) in MSC-related/angiogenesis phenotype/function-related grouping. Collectively, these data indicate that CD146POS cohort show similarities at the protein and transcriptional profile with Crude cohort when cultured in 3D settings *in vitro*.

These phenotypic and molecular differences were also reflected in the immunomodulatory secretory profile upon exposure to inflammatory (TI) or inflammatory/fibrotic (TIC) cues. The overall "signature" response to inflammation in all cohorts involves the upregulation of key immunomodulatory molecules including the T leukocyte recruitment chemokines MCP-2 and RANTES, and the immunosuppressive proteins IP-10 and MIP-1-α, that are directly correlated with the magnitude and cytokine polarity of T cell response *in vivo* [39-41]. In contrast, TIC inflammatory/fibrotic exposure diminished all common secreted molecules resulting in totally distinct secretory phenotypes for the three different cohorts. In terms of biological processes, various categories were highly affected that empower the IFP-MSC spheroids to respond to inflammation/injury by increasing their number, migrating to active sites of damage and altering key cascades known to affect local immune responses.

The immunomodulatory IDO activity and PGE2 secretion were strongly induced by exposure to inflammatory/fibrotic cues as previously reported [23,27,29,42], with the latter secreted in significantly higher levels in the CD146POS cohort. However, these differences were not functionally reflected in immunopotency with IFP-MSC spheroid/PBMC co-cultures. All groups showed a similar gender-independent capacity to abrogate activated PBMC proliferation *in vitro*, indicating that at least via soluble factors CD146-based IFP-MSC selection is not affecting the immunomodulatory functionality of IFP-MSC spheroids. Nevertheless, the comparable PBMC proliferation abrogation observed with Crude, CD146POS and CD146NEG cohorts suggested to us that the 3D environment could be sufficient to induce and/or enhance the immunomodulatory phenotype of IFP-MSC. On the other hand, IFP-MSC spheroids could effectively induce an 'immunomodulatory environment' when co-cultured with synoviocytes exposed to synovitis-mimicking TIC inflammatory/fibrotic cues, similar to a previous report with adipose-derived MSC and OA synoviocytes [43]. IFP-MSC spheroids counterbalanced the synoviocytes induced inflammatory response via secretion of immunomodulatory molecules IP-10, MCP-1, MCP-2, RANTES, low IL-6/IL-8 ratio and articular cartilage degradation inhibitor TIMP-2.

Due to the comparable immunomodulatory functionality of Crude, CD146POS and CD146NEG cohorts in *in vitro* settings, we have evaluated the therapeutic properties of Crude IFP-MSC spheroids *in vivo*. Moreover, IFP-MSC spheroid immunoevasive properties were evident as we did not observe clinical or histological signs of xeno-rejection to the human material. Similar to our previous reports using IFP-MSC in single-cell format [27,28],

IFP-MSC spheroids reverse synovitis/IFP fibrosis

we confirmed that intraarticularly injected spheroids possess strong immunomodulatory/anti-fibrotic capacity resulting in total resolution of synovitis and IFP fibrosis on day 28, as well as degradation of SP. SP is a key modulator of local inflammatory and fibrotic responses as it is involved in the modulation of immune cell proliferation, activation and migration to sites of inflammation, and the expression of recruiting chemokines and adhesion molecules [44,45]. Herein, the reduction or absence of SP^+ fibers in areas of active inflammation and fibrosis for both the synovium and the body of the IFP even from day 7 indicate the strong anti-inflammatory and analgesic IFP-MSC properties *in vivo*. According to our previous findings [27,28], SP degradation both *in vitro* and *in vivo* is driven by a CD10 secretion-dependent degradative mechanism that is apparently strongly effective in IFP-MSC spheroids given their stable and high CD expression. These outcomes are important as SP-secreting sensory nerve fibers predominate over sympathetic ones in anterior knee pain [46-48], whereas SP levels are increased in synovial fluid during joint inflammation [44]. Importantly, Udo et al. showed that intraarticular injection of 1.0 mg MIA in the rat knee leads early to synovitis and IFP fibrosis, and later (on day 28) to severe cartilage erosion [36]. In our study, we confirmed that IFP-MSC intra-articular injected not only result in anti-inflammatory and anti-fibrotic effects but also show strong articular cartilage protective effects.

CONCLUSIONS

In summary, IFP-MSC 3D spheroids exhibit enhanced immunomodulatory phenotypic and transcriptional profiles, reparative growth factor secretion, and anti-inflammatory/anti-fibrotic functional cell signature both *in vitro* and *in vivo*, compared with 2D cultures. These therapeutic properties, when manufactured under minimal-manipulation conditions, facilitates the translation of proof-of-concept data into potential clinical protocols in the treatment of joint disease including synovitis, fat pad fibrosis and consequently OA.

ETHICS APPROVAL AND CONSENT TO PARTICIPATE

Human samples were obtained from elective knee arthroscopy at the Lennar Foundation Medical Center - University of Miami and after provided written informed consent. All procedures were carried out in accordance with relevant guidelines and regulations and following a protocol determined by the University of Miami IRB not as human research (based on the nature of the samples as discarded tissue). Protocol regarding human samples was reviewed and approved by the University of Miami IRB in accordance with the Declaration of Helsinki.

Approval from ethics committee for involving rats was obtained at the University of Miami IACUC. All animal surgeries were conducted in accordance with the Animals (Scientific Procedures) Act 1986 under the IACUC protocol 19-035-LF.

IFP-MSC spheroids reverse synovitis/IFP fibrosis

CONSENT FOR PUBLICATION

Not applicable.

AVAILABILITY OF DATA AND MATERIALS

All data discussed in the paper will be made available to readers upon request.

CONFLICT OF INTEREST

Diego Correa is a paid consultant of Lipogems USA, LLC. Other authors have no conflict of interest.

FUNDING SOURCES

The authors are in gratitude with the Soffer Family Foundation and the DRI Foundation for their generous funding support. These funding sources were not involved in any step of the study design, collection, analysis, or interpretation of the data, or writing of the manuscript.

AUTHOR CONTRIBUTIONS

D.K.: conception and design, collection and assembly of the data, data analysis and interpretation, manuscript writing; M.A.W.: collection and assembly of the data, data analysis and interpretation; T.M.B., L.D.K.: administrative support, final approval of manuscript; D.C.: conception and design, manuscript writing, administrative support, final approval of manuscript.

ACKNOWLEDGEMENTS

The authors want to thank Annie Bowles for her help with the immunopotency assay. The authors want to thank Dylan Greif for his contribution in IFP-MSC sample collection.

References

1 Macchi V, Stocco E, Stecco C et al. The infrapatellar fat pad and the synovial membrane: an anatomo-functional unit [in eng]. J Anat 2018;233(2):146-154.

2 Dragoo JL, Johnson C, McConnell J. Evaluation and treatment of disorders of the infrapatellar fat pad [in eng]. Sports Med 2012;42(1):51-67.

3 Clockaerts S, Bastiaansen-Jenniskens YM, Runhaar J et al. The infrapatellar fat pad should be considered as an active osteoarthritic joint tissue: a narrative review. Osteoarthritis and Cartilage 2010;18(7):876-882.

4 Ioan-Facsinay A, Kloppenburg M. Inflammation and fibrosis in adipose tissue of osteoarthritic joints. Nature Reviews Rheumatology 2017;13:325-326.

5 Kalaitzoglou E, Griffin TM, Humphrey MB. Innate Immune Responses and Osteoarthritis. Current Rheumatology Reports 2017;19(8):45.

6 Remst DFG, Blaney Davidson EN, van der Kraan PM. Unravelling osteoarthritis-related synovial fibrosis: a step closer to solving joint stiffness. Rheumatology 2015;54(11):1954-1963.

7 Tang X, Muhammad H, McLean C et al. Connective tissue growth factor contributes to joint homeostasis and osteoarthritis severity by controlling the matrix sequestration and activation of latent TGFβ. Annals of the Rheumatic Diseases 2018;77(9):1372-1380.

8 Barboza E, Hudson J, Chang WP et al. Profibrotic Infrapatellar Fat Pad Remodeling Without M1 Macrophage Polarization Precedes Knee Osteoarthritis in Mice With Diet-Induced Obesity [in eng]. Arthritis Rheumatol 2017;69(6):1221-1232.

9 Davidson ENB, Vitters EL, Mooren FM et al. Connective tissue growth factor/CCN2 overexpression in mouse synovial lining results in transient fibrosis and cartilage damage. Arthritis & Rheumatism 2006;54(5):1653-1661.

10 Kerna I, Kisand K, Suutre S et al. The ADAM12 is upregulated in synovitis and postinflammatory fibrosis of the synovial membrane in patients with early radiographic osteoarthritis [in eng]. Joint Bone Spine 2014;81(1):51-56.

11 Benito MJ, Veale DJ, FitzGerald O et al. Synovial tissue inflammation in early and late osteoarthritis [in eng]. Annals of the rheumatic diseases 2005;64(9):1263-1267.

12 Felson DT, Niu J, Neogi T et al. Synovitis and the risk of knee osteoarthritis: the MOST Study [in eng]. Osteoarthritis and cartilage 2016;24(3):458-464.

13 Mathiessen A, Conaghan PG. Synovitis in osteoarthritis: current understanding with therapeutic implications [in eng]. Arthritis research & therapy 2017;19(1):18.

14 Scanzello CR, Goldring SR. The role of synovitis in osteoarthritis pathogenesis [in eng]. Bone 2012;51(2):249-257.

15 Sokolove J, Lepus CM. Role of inflammation in the pathogenesis of osteoarthritis: latest findings and interpretations [in eng]. Therapeutic advances in musculoskeletal disease 2013;5(2):77-94.

16 Attur M, Samuels J, Krasnokutsky S et al. Targeting the synovial tissue for treating osteoarthritis (OA): where is the evidence? Best Practice & Research Clinical Rheumatology 2010;24(1):71-79.

17 Karsdal MA, Michaelis M, Ladel C et al. Disease-modifying treatments for osteoarthritis (DMOADs) of the knee and hip: lessons learned from failures and opportunities for the future [in eng]. Osteoarthritis Cartilage 2016;24(12):2013-2021.

18 Garza JR, Campbell RE, Tjoumakaris FP et al. Clinical Efficacy of Intra-articular Mesenchymal Stromal Cells for the Treatment of Knee Osteoarthritis: A Double-Blinded Prospective Randomized Controlled Clinical Trial [in eng]. Am J Sports Med 2020;48(3):588-598.

19 Matas J, Orrego M, Amenabar D et al. Umbilical Cord-Derived Mesenchymal Stromal Cells (MSCs) for Knee Osteoarthritis: Repeated MSC Dosing Is Superior to a Single MSC Dose and to Hyaluronic Acid in a Controlled Randomized Phase I/II Trial [in eng]. Stem cells translational medicine 2019;8(3):215-224.

20 Soler R, Orozco L, Munar A et al. Final results of a phase I-II trial using ex vivo expanded autologous Mesenchymal Stromal Cells for the treatment of osteoarthritis of the knee confirming safety and suggesting cartilage regeneration [in eng]. Knee 2016;23(4):647-654.

21 Caplan Arnold I, Correa D. The MSC: An Injury Drugstore. Cell Stem Cell 2011;9(1):11-15.

22 Waterman RS, Tomchuck SL, Henkle SL et al. A New Mesenchymal Stem Cell (MSC) Paradigm: Polarization into a Pro-Inflammatory MSC1 or an Immunosuppressive MSC2 Phenotype. Plos One 2010;5(4):e10088.

23 Bernardo Maria E, Fibbe Willem E. Mesenchymal Stromal Cells: Sensors and Switchers of Inflammation. Cell Stem Cell 2013;13(4):392-402.

24 Garcia J, Wright K, Roberts S et al. Characterisation of synovial fluid and infrapatellar fat pad derived mesenchymal stromal cells: The influence of tissue source and inflammatory stimulus [in eng]. Sci Rep 2016;6:24295.

25 Skalska U, Kontny E. Adipose-derived mesenchymal stem cells from infrapatellar fat pad of patients with rheumatoid arthritis and osteoarthritis have comparable immunomodulatory properties [in eng]. Autoimmunity 2016;49(2):124-131.

26 Dragoo JL, Samimi B, Zhu M et al. Tissue-engineered cartilage and bone using stem cells from human infrapatellar fat pads. The Journal of Bone and Joint Surgery British volume 2003;85-B(5):740-747.

27 Kouroupis D, Bowles AC, Willman MA et al. Infrapatellar fat pad-derived MSC response to inflammation and fibrosis induces an immunomodulatory phenotype involving CD10-mediated Substance P degradation. Scientific Reports 2019;9(1):10864.

28 Kouroupis D, Bowles AC, Best TM et al. CD10/neprilysin enrichment in infrapatellar fat pad-derived MSC under regulatory-compliant conditions: implications for efficient synovitis and fat pad fibrosis reversal. The American Journal of Sports Medicine 2020:in press.
29 Kouroupis D, Bowles AC, Greif DN et al. Regulatory-compliant conditions during cell product manufacturing enhance infrapatellar fat pad-derived mesenchymal stem/stromal cells immunomodulatory properties in vitro. Cytotherapy 2020:in press.
30 Bowles AC, Kouroupis D, Willman MA et al. Signature quality attributes of CD146+ mesenchymal stem/stromal cells correlate with high therapeutic and secretory potency. Stem Cells 2020;38(8):1034-1049.
31 Churchman SM, Ponchel F, Boxall SA et al. Transcriptional profile of native CD271+ multipotential stromal cells: Evidence for multiple fates, with prominent osteogenic and Wnt pathway signaling activity. Arthritis & Rheumatism 2012;64(8):2632-2643.
32 Jones E, English A, Churchman SM et al. Large-scale extraction and characterization of CD271+ multipotential stromal cells from trabecular bone in health and osteoarthritis: implications for bone regeneration strategies based on uncultured or minimally cultured multipotential stromal cells [; Research Support, Non-U.S. Gov't] [in English]. Arthritis Rheum 2010;62(7):1944-1954.
33 Petrenko Y, Syková E, Kubinová Š. The therapeutic potential of three-dimensional multipotent mesenchymal stromal cell spheroids. Stem Cell Research & Therapy 2017;8:94.
34 Kouroupis D, Sanjurjo-Rodriguez C, Jones E et al. Mesenchymal Stem Cell Functionalization for Enhanced Therapeutic Applications. Tissue Engineering Part B: Reviews 2018;25(1):55-77.
35 Kouroupis D, Kyrkou A, Triantafyllidi E et al. Generation of stem cell-based bioartificial anterior cruciate ligament (ACL) grafts for effective ACL rupture repair. Stem Cell Research 2016;17(2):448-457.
36 Udo M, Muneta T, Tsuji K et al. Monoiodoacetic acid induces arthritis and synovitis in rats in a dose- and time-dependent manner: proposed model-specific scoring systems. Osteoarthritis and Cartilage 2016;24(7):1284-1291.
37 Bartosh TJ, Ylostalo JH, Mohammadipoor A et al. Aggregation of human mesenchymal stromal cells (MSCs) into 3D spheroids enhances their antiinflammatory properties. Proceedings of the National Academy of Sciences 2010;107(31):13724-13729.
38 Guo L, Zhou Y, Wang S et al. Epigenetic changes of mesenchymal stem cells in three-dimensional (3D) spheroids. Journal of Cellular and Molecular Medicine 2014;18(10):2009-2019.
39 Chinnadurai R, Rajan D, Qayed M et al. Potency Analysis of Mesenchymal Stromal Cells Using a Combinatorial Assay Matrix Approach. Cell Reports 2018;22(9):2504-2517.
40 Loetscher P, Seitz M, Clark-Lewis I et al. Monocyte chemotactic proteins MCP-1, MCP-2, and MCP-3 are major attractants for human CD4+ and CD8+ T lymphocytes [in eng]. FASEB J 1994;8(13):1055-1060.
41 Luther SA, Cyster JG. Chemokines as regulators of T cell differentiation. Nature Immunology 2001;2(2):102-107.
42 Waterman RS, Henkle SL, Betancourt AM. Mesenchymal Stem Cell 1 (MSC1)-Based Therapy Attenuates Tumor Growth Whereas MSC2-Treatment Promotes Tumor Growth and Metastasis. PLoS ONE 2013;7(9):e45590.
43 Manferdini C, Maumus M, Gabusi E et al. Adipose-Derived Mesenchymal Stem Cells Exert Antiinflammatory Effects on Chondrocytes and Synoviocytes From Osteoarthritis Patients Through Prostaglandin E2. Arthritis & Rheumatism 2013;65(5):1271-1281.
44 Mashaghi A, Marmalidou A, Tehrani M et al. Neuropeptide substance P and the immune response [in eng]. Cellular and molecular life sciences : CMLS 2016;73(22):4249-4264.
45 Spitsin S, Meshki J, Winters A et al. Substance P–mediated chemokine production promotes monocyte migration. Journal of Leukocyte Biology 2017;101(4):967-973.
46 Lehner B, Koeck FX, Capellino S et al. Preponderance of sensory versus sympathetic nerve fibers and increased cellularity in the infrapatellar fat pad in anterior knee pain patients after primary arthroplasty. Journal of Orthopaedic Research 2008;26(3):342-350.
47 Bohnsack M, Meier F, Walter GF et al. Distribution of substance-P nerves inside the infrapatellar fat pad and the adjacent synovial tissue: a neurohistological approach to anterior knee pain syndrome. Archives of Orthopaedic and Trauma Surgery 2005;125(9):592-597.
48 Koeck FX, Schmitt M, Baier C et al. Predominance of synovial sensory nerve fibers in arthrofibrosis following total knee arthroplasty compared to osteoarthritis of the knee. Journal of Orthopaedic Surgery and Research 2016;11(1):25.

Figure Legends

Graphical abstract: In this proof-of-concept study, IFP-MSC cultured in 3D spheroid conditions show superior paracrine and immunoregulatory properties than in 2D cultures *in vitro*, while inducing Substance P degradation and inflammation/fibrosis reversal *in vivo*. The resulting fine-tuned, cell-based product has potential future utilization as a novel minimally-invasive therapy for enhanced OA treatment.

Figure 1: IFP-MSC spheroid immunophenotypic profile and tripotentiality. (A) In 2D settings, Crude IFP-MSC show stable MSC-related phenotypic profile with high expression levels for CD44 and CD90 markers and increased donor-to-donor variability in CD10, CD146, and CXCR4 expression levels. (B and C) Upon seeding in gas-permeable culture plates, Crude IFP-MSC can generate multiple sized spheroids (100-300μm) with enhanced expression of CD90, CXCR4, CD10, and NG2. CD146 and CD44 show variable expression levels between spheroids. (D) IFP-MSC spheroids can efficiently differentiate towards chondrogenic, osteogenic and adipogenic lineages after specific induction in gas-permeable plates. Quantitative molecular profiling showed that differentiation-related markers in induced IFP-MSC spheroids were increased compared to non-induced cultures, indicating their mature status. All experiments (n=3) were performed independently and data are presented as mean ± SD (*$p<0.05$).

Figure 2: Molecular and secretory profiling of 2-D IFP-MSC and IFP-MSC spheroids. (A) Molecular profiling of non-induced IFP-MSC spheroids versus non-induced 2-D IFP-MSC cultures revealed that 49 out of 90 genes tested were higher expressed in IFP-MSC spheroids with 24 genes being more than two-fold higher. Genes tested were grouped in phenotype/function-related cohorts. (B and C) The secretory profile of inflammation-related cytokines revealed that non-induced IFP-MSC spheroids show significantly ($p<0.05$) higher secretion of 13 and lower secretion of 5 (IL-6, IL-6sR, IL-16, MIP-1-β, TNF-α) out of 40 secreted proteins tested compared to naïve 2-D IFP-MSC cultures. In addition, non-induced IFP-MSC spheroids show significantly ($p<0.05$) higher secretion of 36 out of 41 secreted protein tested. Heat maps colours are assigned according to a molecule concentration relative scale, from 0 to 10,000. All experiments were performed independently (n=2).

Figure 3: Immunophenotype and molecular profile of CD146-selected IFP-MSC spheroids. (A) Upon seeding in gas-permeable culture plates, CD146POS IFP-MSC spheroids show as expected higher expression levels of CD146 (451±4 AU vs 241±18 AU) and higher expression levels of NG2 (362±178 AU vs 287±22 AU), whereas CD146NEG IFP-MSC spheroids show higher expression levels of CD10 (253±27 AU vs 164±13 AU) and CXCR4 (227±3 AU vs 140±14 AU). (B) Molecular profiling of CD146POS versus CD146NEG IFP-MSC spheroids revealed that 55 out of 90 genes tested were higher expressed in CD146POS IFP-MSC spheroids with

12 genes being more than two-fold higher (*MCAM, HGF, ALPL, DLX5, NES, MMP13, CD200, COL1A1, FZD9, PDGFRB, HIC1*). Genes tested were grouped in phenotype/function-related cohorts. (C) 26 genes are shared between Crude and CD146POS spheroids, indicating similarities in their molecular signatures. However, upon TI- or TIC- induction most of the immunoregulatory-related genes tested show up-regulated expression levels in CD146POS spheroids. All experiments were performed independently (n=3).

Figure 4: Secretory profiling of Crude and CD146-selected IFP-MSC spheroids with and without exposure to inflammatory/fibrotic cues. (A and B) Crude and CD146-selected IFP-MSC spheroids show similar inflammation-related secretory profiles both in non-induced and TI- or TIC-induced conditions. However, their secretory profiles of reparative growth factors were distinct and characterized by the secretion of different numbers and types of proteins. Heat maps colours are assigned according to a molecule concentration relative scale, from 0 to 10,000 (n=2). (C) In both TI- and TIC-induced conditions, CD146POS IFP-MSC spheroids show higher number of secreted proteins. Among the proteins with up-regulated secretion levels 6 and none proteins are commonly shared between the three different cohorts (crude, CD146POS, CD146NEG) after TI and TIC induction, respectively. Venn diagram showing shared proteins amongst the three different cohorts (Crude, CD146POS, CD146NEG) after TI and TIC induction. All experiments were performed independently (n=2). (D) In non-induced cohorts IDO secretion is almost absent whereas PGE2 secretion is evident in all three cohorts. TIC induction result in increased IDO and PGE2 secretion levels (*$p<0.05$, n=3).

Figure 5: Immunomodulatory functionality of Crude IFP-MSC spheroids. () CFSE-labeled, PMA/IO-activated human PBMC showed a proliferation of ~91.2% for male PBMC donors and of ~89.9% for female PBMC donors, which was suppressed in a PBMC gender-dependent manner by co-culture with non-induced Crude or CD146-selected IFP-MSC spheroids (*$p<0.05$, n=3). (B) In both non-induced and TIC-induced SYN, non-induced Crude IFP-MSC spheroids can effectively form explant-cultures on synoviocyte monolayer whereas TIC induction of SYN significantly (*p<0.05) up-regulate inflammatory genes such as CD13 and PD-1. (C) SYN/IFP-MSC spheroid co-cultures resulted in significantly (*p<0.05) higher secretion of immunomodulatory proteins (IL-6, IL-8, IP-10, MCP-1, MCP2, RANTES, TIMP-2) compared to TIC-induced SYN alone. All experiments were performed independently (n=3).

Figure 6: IFP-MSC spheroids effectively reverse synovitis and IFP fibrosis *in vivo.* Schematic indicating the generation of acute synovitis/IFP fibrosis rat model, therapeutic intervention and chronological evaluation. (A and B) Hematoxylin/Eosin staining (top 2 panels), Masson's trichrome staining (middle two panels) and Substance P immunolocalization (lower 2 panels) in sagitally-sectioned knees of representative rats for healthy control, injected only with MIA or with both MIA and IFP-MSC spheroids. Compared with only MIA injected

group, which showed a significant synovitis and IFP fibrosis with cellular infiltrates, a striking correlation was found between IFP-MSC spheroid treatment and the effect reducing inflammation and fibrosis after 3 and 25 days of a single intra-articular IFP-MSC injection. (C) After MIA injection, all animals developed OA changes that resulted in OA lesions on day 28. IFP-MSC spheroid injection group didn't show any major OA lesion development whereas articular cartilage sGAG content was preserved which was evident by the strong toluidine blue staining.

Supplementary Figure 1: Molecular evaluation of IFP-MSC spheroids. (A) *CD146* gene expression levels show not only high up-regulation in 3D settings compared to 2D cultures but also higher expression in CD146NEG IFP-MSC spheroids. (B) Upon TI- or TIC- induction most of the immunomodulatory-related genes tested show up-regulated expression levels in CD146POS spheroids. All experiments were performed independently (n=3).

Supplementary Figure 2: Tables show the number of proteins significantly different between the three different cohorts (Crude, CD146POS, CD146NEG) upon TI or TIC induction compared to non-induced cultures.

Supplementary Figure 3: Interactome of proteins significantly up-regulated in TI or TIC conditions. All secreted proteins appeared interconnected at least through one association (except PIGF when present) and the K-means clustering networks demonstrated elevated protein-protein interaction (PPI) enrichment (p-value <1.0e-16) and an average local clustering coefficient >0.7 indicating that the proteins used are at least partially biologically connected. (A) In TI-induced IFP-MSC spheroids all subpopulation cohorts revealed overall similar biological processes. Crude TI-induced cohort showed higher involvement in all tested biological processes except positive regulation of cell population proliferation and angiogenesis, which showed significantly higher involvement in TI-induced CD146POS cohort (5.5% and 16.5% higher respectively) (Supplementary Figure 2A, left radar graph). (B) In TIC-induced IFP-MSC spheroids, Crude cohort showed higher involvement in 4 out of 7 biological processes tested. Compared to TI induction, TIC induction significantly decreased the angiogenesis biological process involvement in crude cohort (from 14 to 0%) and significantly increased its involvement in CD146POS cohort (from 30.7 to 41.7%) (A and B) Overall, in both TI- and TIC-induced IFP-MSC spheroids, CD146POS cohort showed significantly stronger protein involvement in 4 out of 8 KEGG reactome pathways (MAPK, PI3K-Akt, Ras, and Rap1 signaling pathways) compared to other cohorts.

Graphical abstract

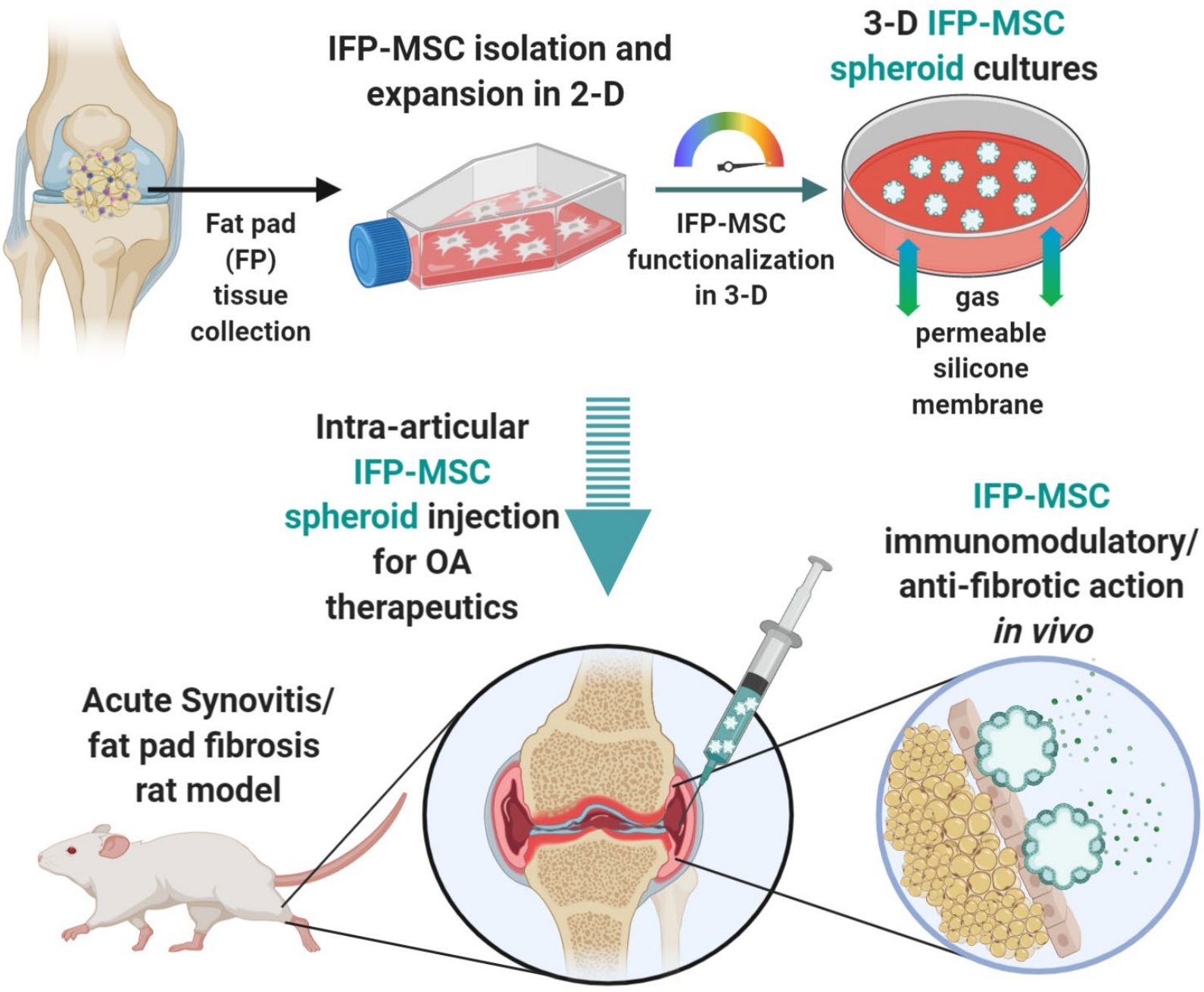

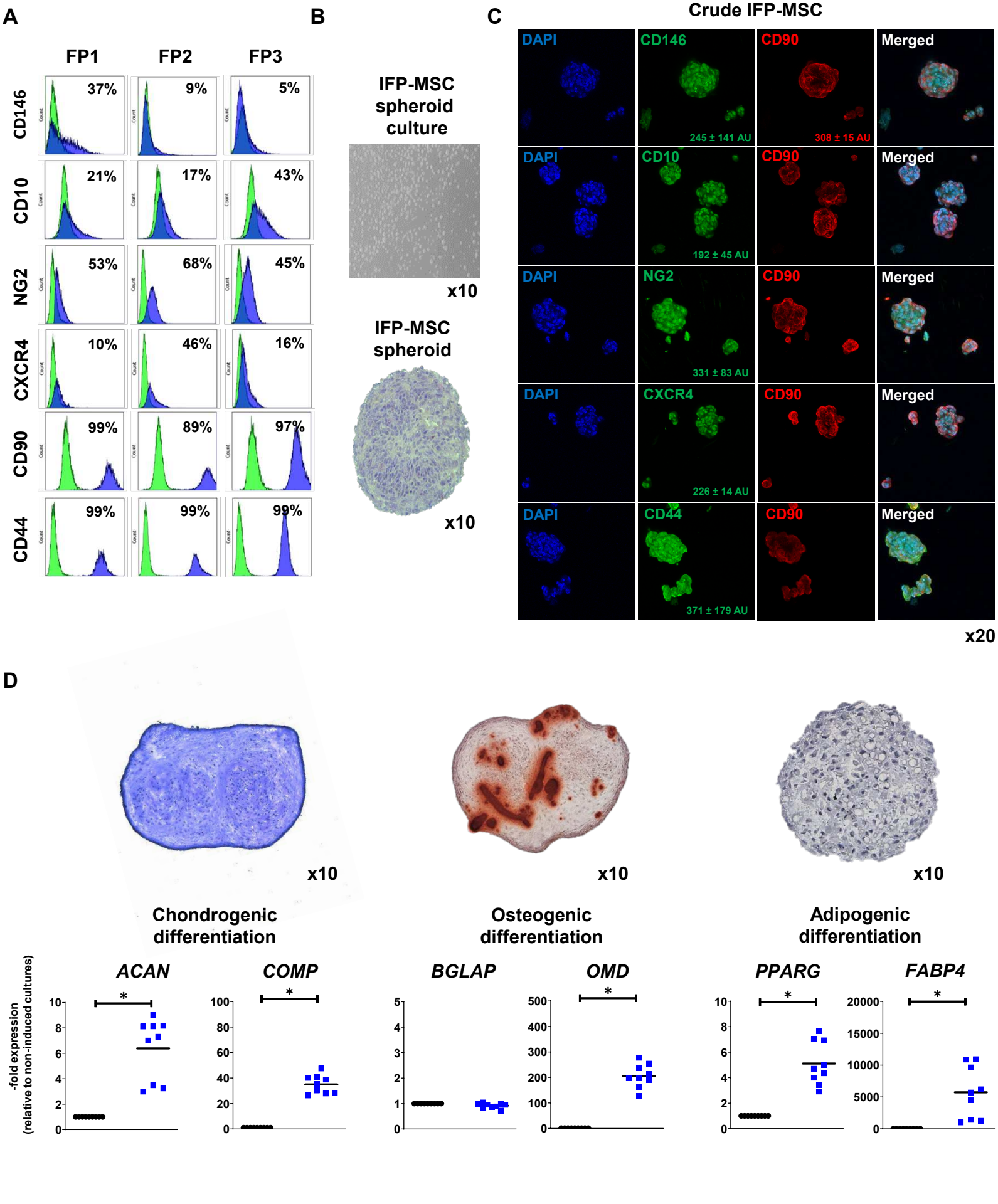
A
FP1
FP2
FP3
CD146
37%
9%
5%
CD10
21%
17%
43%
NG2
53%
68%
45%
CXCR4
10%
46%
16%
CD90
99%
89%
97%
CD44
99%
99%
99%
B
IFP-MSC spheroid culture
x10
IFP-MSC spheroid
x10
C
Crude IFP-MSC
DAPI
CD146
245 ± 141 AU
CD90
308 ± 15 AU
Merged
DAPI
CD10
192 ± 45 AU
CD90
Merged
DAPI
NG2
331 ± 83 AU
CD90
Merged
DAPI
CXCR4
226 ± 14 AU
CD90
Merged
DAPI
CD44
371 ± 179 AU
CD90
Merged
x20
D
x10
x10
x10
Chondrogenic differentiation
Osteogenic differentiation
Adipogenic differentiation
-fold expression (relative to non-induced cultures)
ACAN
COMP
BGLAP
OMD
PPARG
FABP4
*

A

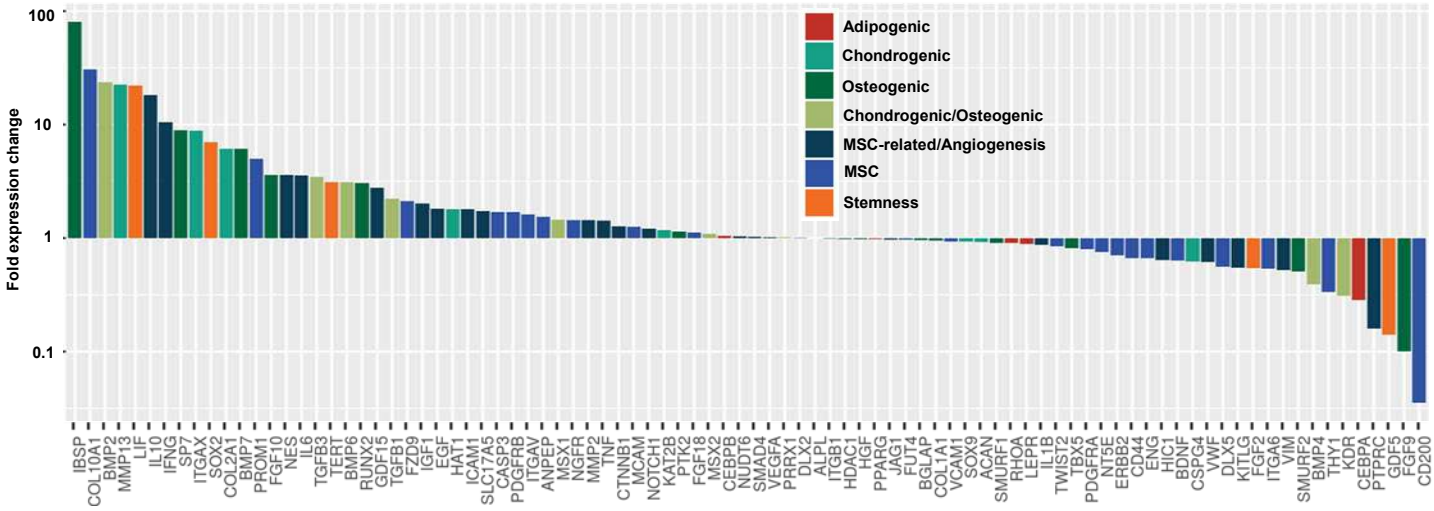

Classification	Genes	Median Fold Change (3D spheroids to 2D cultures)	P-Value
Stemness	LIF, SOX2, TERT, FGF2, GDF5	2.69735	0.4137
Chondrogenic	MMP13, ITGAX, COL2A1, HAT1, KAT2B, SOX9, ACAN, CSPG4	1.69247	0.55794
MSC-related/ Angiogenesis	IL10, IFNG, NES, IL6, GDF15, IGF1, EGF, ICAM1, SLC17A5, MMP2, TNF, CTNNB1, NOTCH1, NUDT6, SMAD4, VEGFA, ITGB1, HGF, JAG1, IL1B, HIC1, VWF, KITLG, VIM, PTPRC	1.28867	0.28437
Chondrogenic / Osteogenic	BMP2, TGFB3, BMP6, TGFB1, MSX1, MSX2, PRRX1, BMP4, KDR	1.26607	0.91703
Osteogenic	IBSP, SP7, BMP7, FGF10, RUNX2, PTK2, ALPL, HDAC1, BGLAP, COL1A1, SMURF1, TBX5, SMURF2, FGF9	1.10396	0.03289
Adipogenic	CEBPB, PPARG, RHOA, LEPR, CEBPA	0.90238	0.36788
MSC	COL10A1, PROM1, FZD9, CASP3, PDGFRB, ITGAV, ANPEP, NGFR, MCAM, FGF18, DLX2, FUT4, VCAM1, TWIST2, PDGFRA, NT5E, ERBB2, CD44, ENG, BDNF, DLX5, ITGA6, THY1, CD200	0.86973	0.28865

B

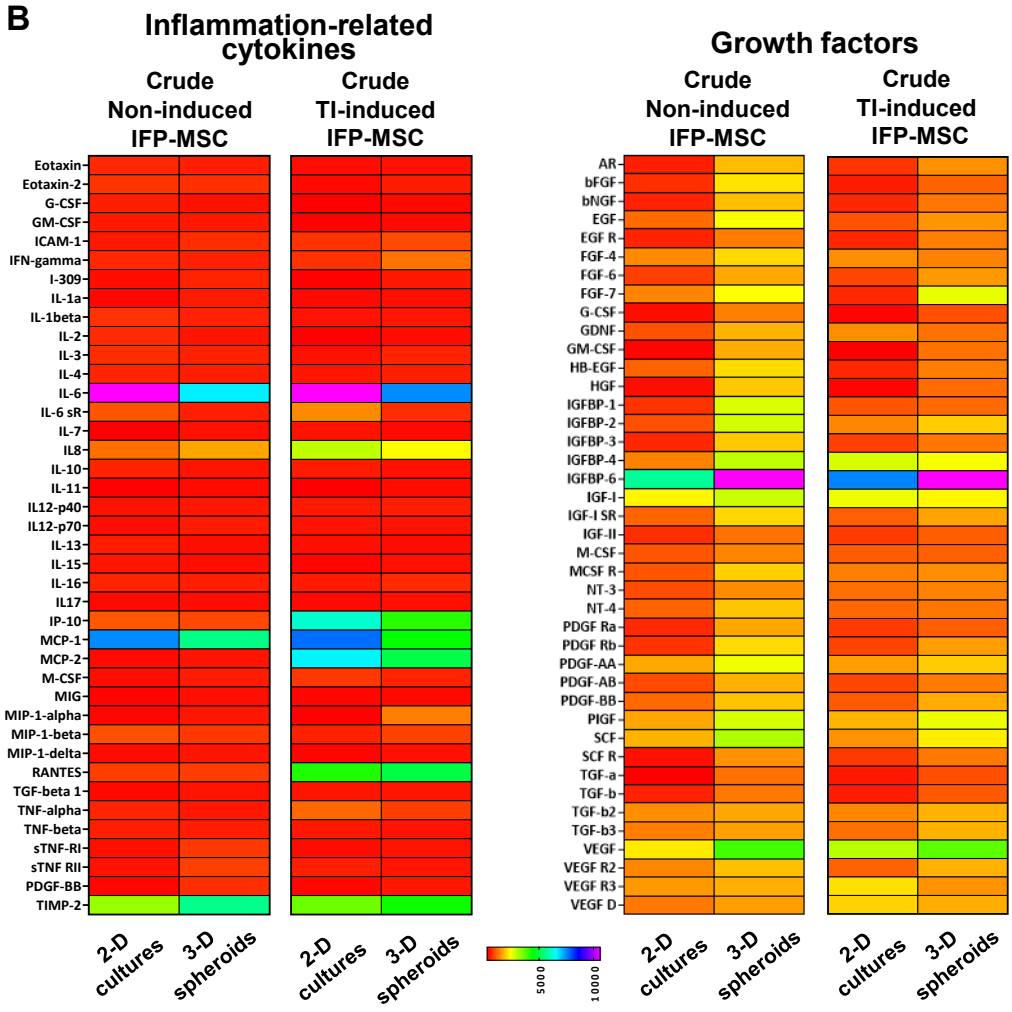

C

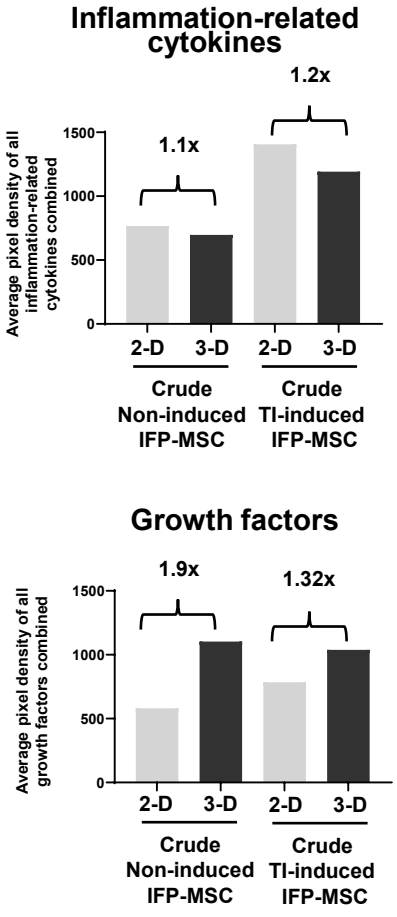

Figure 3

A

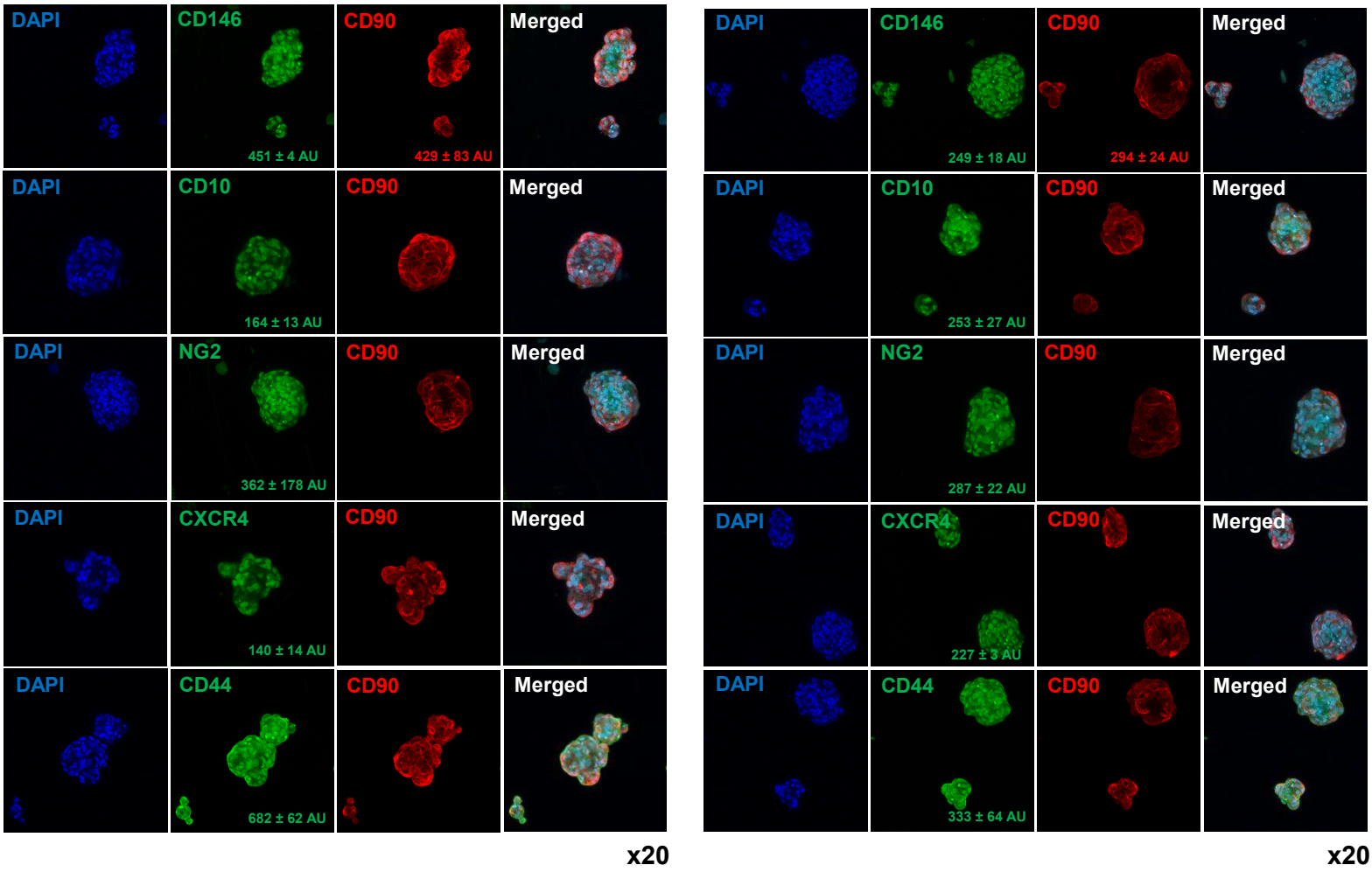

B

Classification	Genes (high to low expressed)	Median Fold Change (CD146POS to CD146NEG spheroids)	P-Value
Chondrogenic	MMP13, COL2A1, ACAN, CSPG4, SOX9, KAT2B, HAT1, ITGAX	1.29896	0.96834
MSC-related/ Angiogenesis	HGF, NES, HIC1, NOTCH1, VEGFA, VIM, KITLG, IFNG, PTPRC, VWF, CTNNB1, NUDT6, ITGB1, IL10, SMAD4, JAG1, IL6, IL1B, SLC17A5, TNF, IGF1, MMP2, ICAM1, GDF15, EGF	1.08671	0.97092
Osteogenic	ALPL, COL1A1, IBSP SP7, SMURF2, TBX5, HDAC1, SMURF1, PTK2, RUNX2, BGLAP, BMP7, FGF9, FGF10	0.99308	0.83883
MSC	MCAM, DLX5, CD200, FZD9, PDGFRB, PROM1, BDNF, ENG, NT5E, PDGFRA, ERBB2, ANPEP, THY1, TWIST2, ITGAV, NGFR, CD44, FUT4, ITGA6, FGF18, DLX2, CASP3, COL10A1, VCAM1	0.97572	0.14054
Adipogenic	RHOA, PPARG, CEBPB, LEPR, CEBPA	0.86597	0.53186
Chondrogenic / Osteogenic	TGFB3, BMP6, TGFB1, MSX1, PRRX1, BMP2, MSX2, BMP4, KDR	0.83926	0.32845
Stemness	LIF, TERT, GDF5, FGF2, SOX2	0.81718	0.62319

C

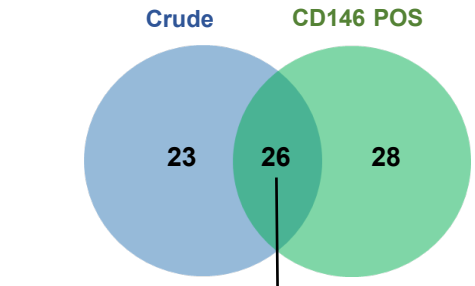

Commonly up-regulated genes in Crude and CD146POS IFP-MSC Spheroids

MMP13	IL10
COL2A1	IFNG
HAT1	NES
KAT2B	CTNNB1
TGFB3	NOTCH1
BMP6	NUDT6
TGFB1	SMAD4
PROM1	VEGFA
FZD9	IBSP
PDGFRB	SP7
ANPEP	RUNX2
MCAM	PTK2
	LIF
	TERT

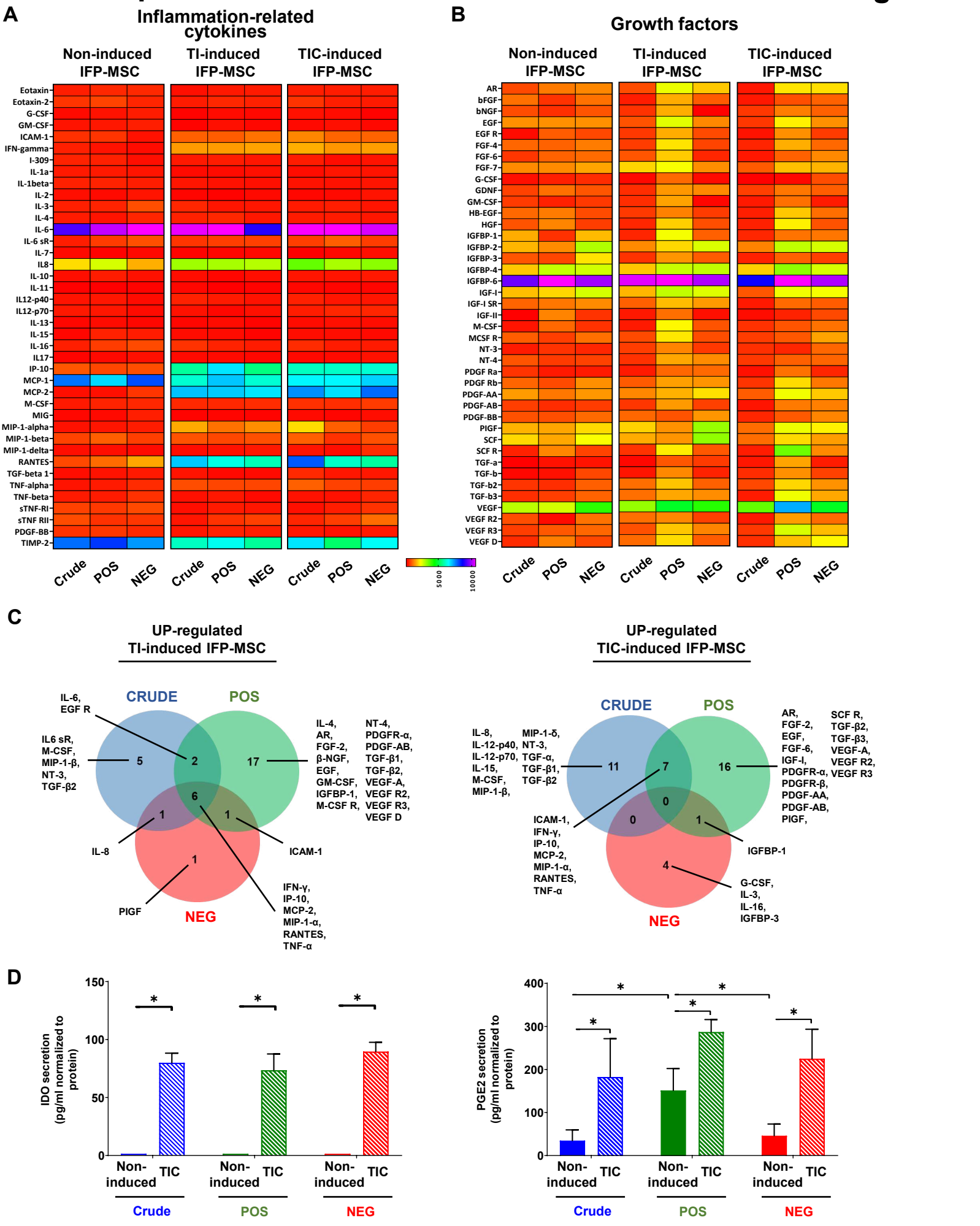
A
Inflammation-related cytokines
Non-induced IFP-MSC
TI-induced IFP-MSC
TIC-induced IFP-MSC
Eotaxin
Eotaxin-2
G-CSF
GM-CSF
ICAM-1
IFN-gamma
I-309
IL-1a
IL-1beta
IL-2
IL-3
IL-4
IL-6
IL-6 sR
IL-7
IL8
IL-10
IL-11
IL12-p40
IL12-p70
IL-13
IL-15
IL-16
IL17
IP-10
MCP-1
MCP-2
M-CSF
MIG
MIP-1-alpha
MIP-1-beta
MIP-1-delta
RANTES
TGF-beta 1
TNF-alpha
TNF-beta
sTNF-RI
sTNF RII
PDGF-BB
TIMP-2
Crude
POS
NEG
5000
10000
B
Growth factors
Non-induced IFP-MSC
TI-induced IFP-MSC
TIC-induced IFP-MSC
AR
bFGF
bNGF
EGF
EGF R
FGF-4
FGF-6
FGF-7
G-CSF
GDNF
GM-CSF
HB-EGF
HGF
IGFBP-1
IGFBP-2
IGFBP-3
IGFBP-4
IGFBP-6
IGF-I
IGF-I SR
IGF-II
M-CSF
MCSF R
NT-3
NT-4
PDGF Ra
PDGF Rb
PDGF-AA
PDGF-AB
PDGF-BB
PIGF
SCF
SCF R
TGF-a
TGF-b
TGF-b2
TGF-b3
VEGF
VEGF R2
VEGF R3
VEGF D
C
UP-regulated TI-induced IFP-MSC
CRUDE
POS
NEG
IL-6, EGF R
IL6 sR, M-CSF, MIP-1-β, NT-3, TGF-β2
5
2
17
6
1
1
1
IL-8
ICAM-1
PIGF
IL-4, AR, FGF-2, β-NGF, EGF, GM-CSF, IGFBP-1, M-CSF R,
NT-4, PDGFR-α, PDGF-AB, TGF-β1, TGF-β2, VEGF-A, VEGF R2, VEGF R3, VEGF D
IFN-γ, IP-10, MCP-2, MIP-1-α, RANTES, TNF-α
UP-regulated TIC-induced IFP-MSC
CRUDE
POS
NEG
IL-8, IL-12-p40, IL-12-p70, IL-15, M-CSF, MIP-1-β,
MIP-1-δ, NT-3, TGF-α, TGF-β1, TGF-β2
11
7
16
0
0
1
4
ICAM-1, IFN-γ, IP-10, MCP-2, MIP-1-α, RANTES, TNF-α
AR, FGF-2, EGF, FGF-6, IGF-I, PDGFR-α, PDGFR-β, PDGF-AA, PDGF-AB, PIGF,
SCF R, TGF-β2, TGF-β3, VEGF-A, VEGF R2, VEGF R3
IGFBP-1
G-CSF, IL-3, IL-16, IGFBP-3
D
IDO secretion (pg/ml normalized to protein)
150
100
50
0
*
Non-induced
TIC
Crude
POS
NEG
PGE2 secretion (pg/ml normalized to protein)
400
300
200
100
0
*

Figure 5

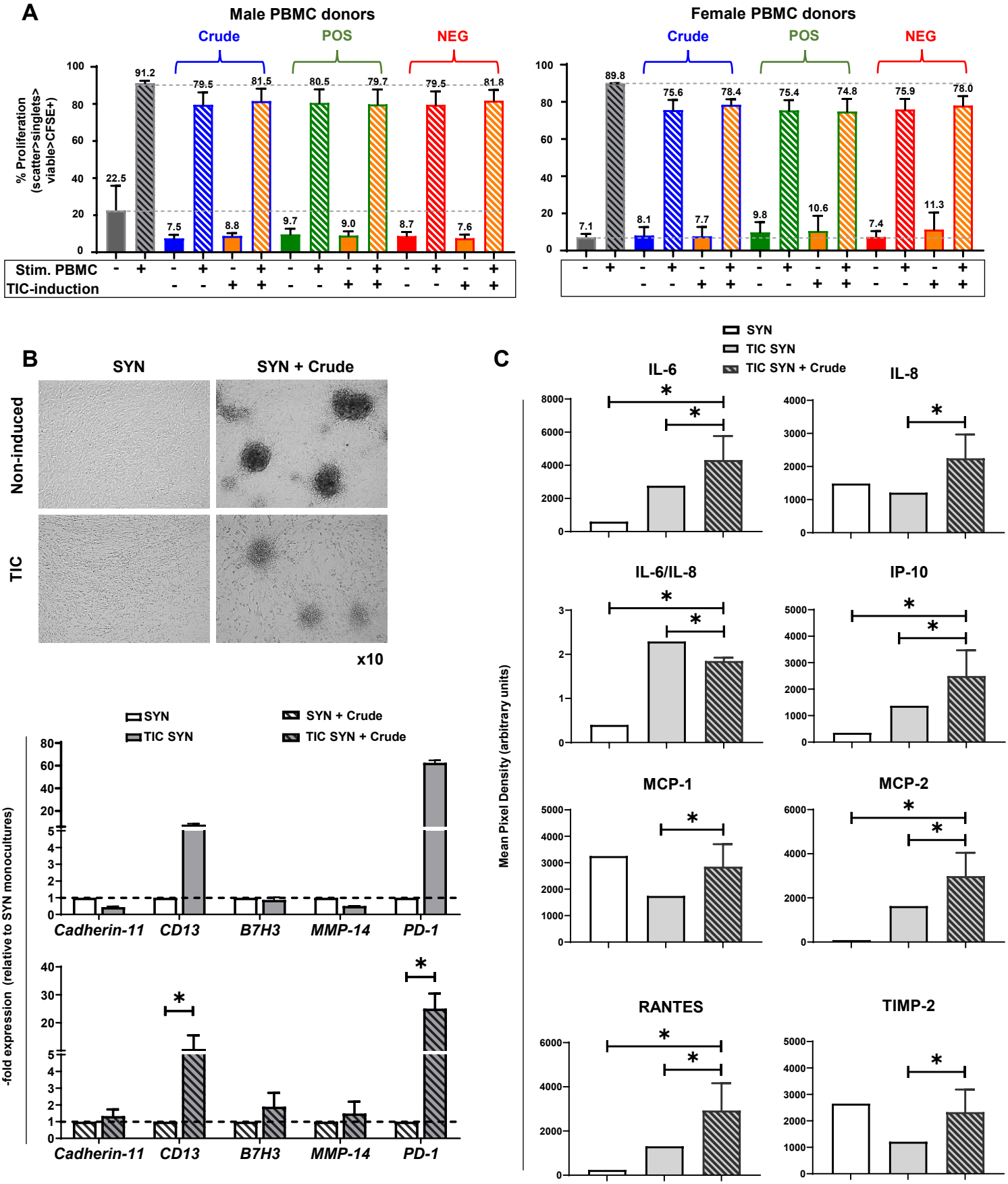
A
Male PBMC donors
Female PBMC donors
Crude
POS
NEG
% Proliferation (scatter>singlets> viable>CFSE+)
Stim. PBMC
TIC-induction
B
SYN
SYN + Crude
Non-induced
TIC
x10
SYN
TIC SYN
SYN + Crude
TIC SYN + Crude
-fold expression (relative to SYN monocultures)
Cadherin-11
CD13
B7H3
MMP-14
PD-1
C
SYN
TIC SYN
TIC SYN + Crude
Mean Pixel Density (arbitrary units)
IL-6
IL-8
IL-6/IL-8
IP-10
MCP-1
MCP-2
RANTES
TIMP-2

Figure 6

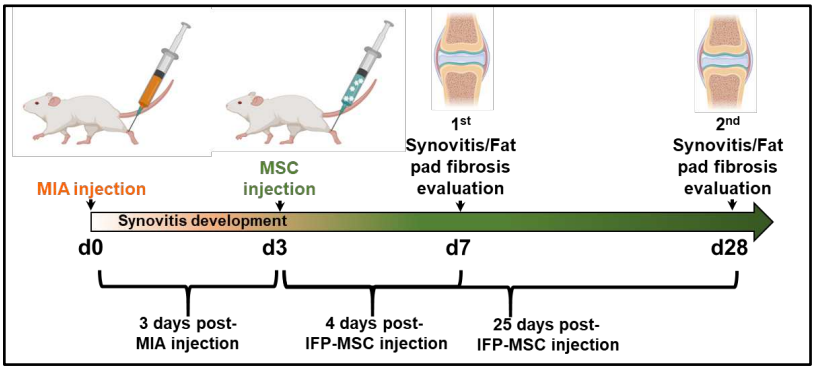
MIA injection
MSC injection
1st Synovitis/Fat pad fibrosis evaluation
2nd Synovitis/Fat pad fibrosis evaluation
Synovitis development
d0
d3
d7
d28
3 days post-MIA injection
4 days post-IFP-MSC injection
25 days post-IFP-MSC injection

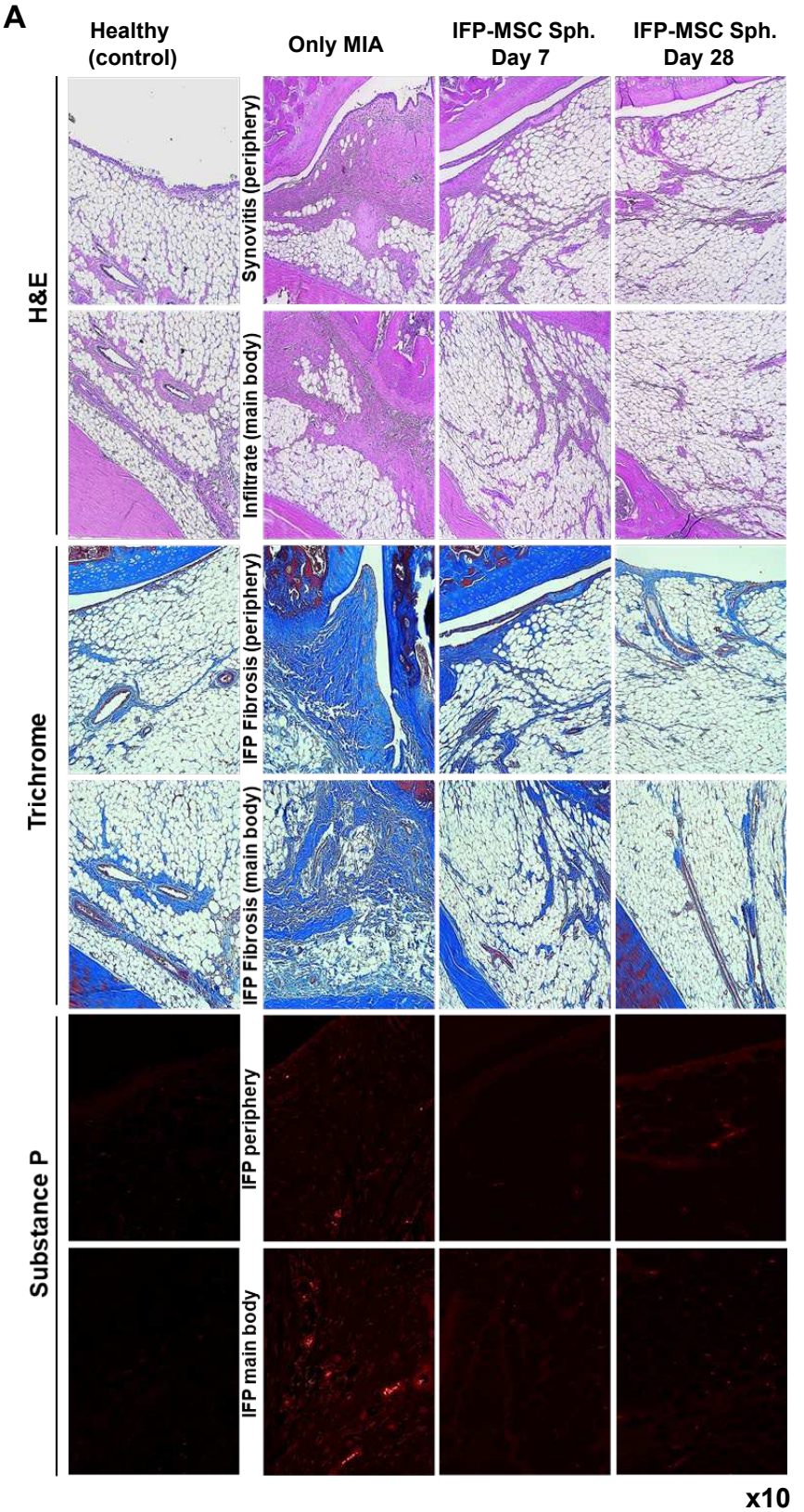
A
Healthy (control)
Only MIA
IFP-MSC Sph. Day 7
IFP-MSC Sph. Day 28
H&E
Synovitis (periphery)
Infiltrate (main body)
Trichrome
IFP Fibrosis (periphery)
IFP Fibrosis (main body)
Substance P
IFP periphery
IFP main body
x10

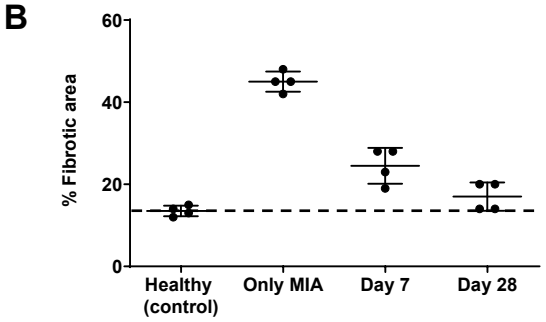
B
% Fibrotic area
60
40
20
0
Healthy (control)
Only MIA
Day 7
Day 28

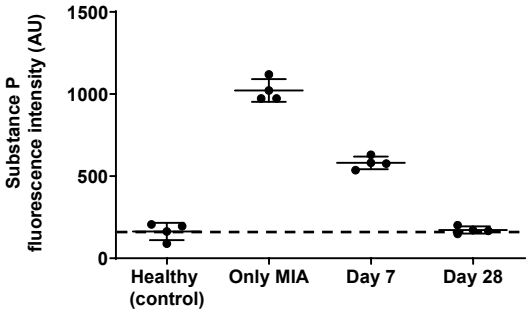
Substance P fluorescence intensity (AU)
1500
1000
500
0
Healthy (control)
Only MIA
Day 7
Day 28

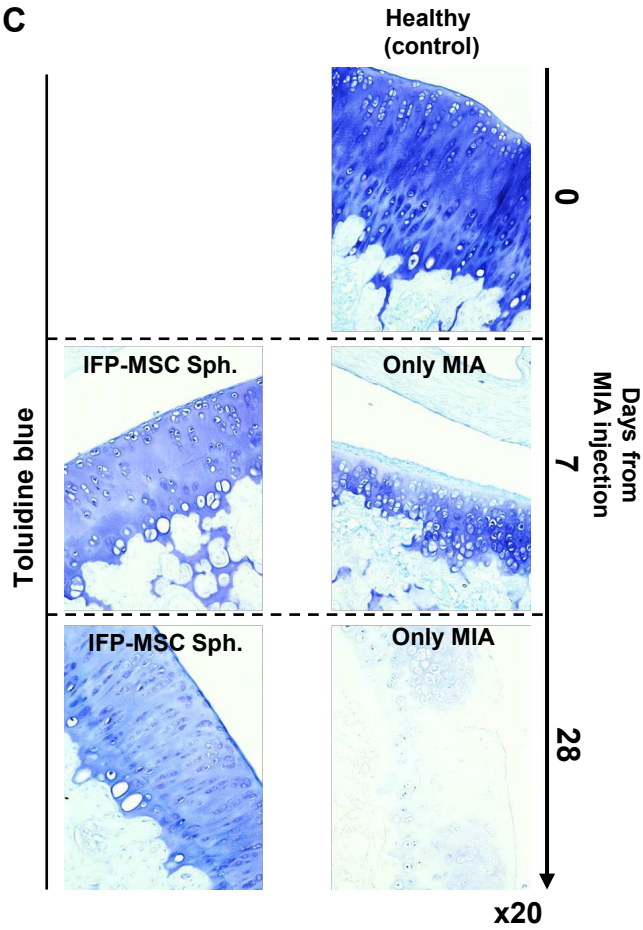
C
Healthy (control)
Toluidine blue
IFP-MSC Sph.
Only MIA
IFP-MSC Sph.
Only MIA
0
7
28
Days from MIA injection
x20

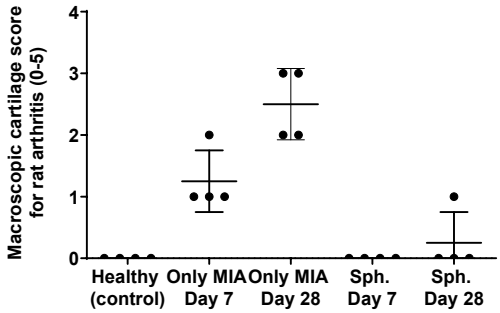
Macroscopic cartilage score for rat arthritis (0-5)
4
3
2
1
0
Healthy (control)
Only MIA Day 7
Only MIA Day 28
Sph. Day 7
Sph. Day 28

Supplementary Figure 1

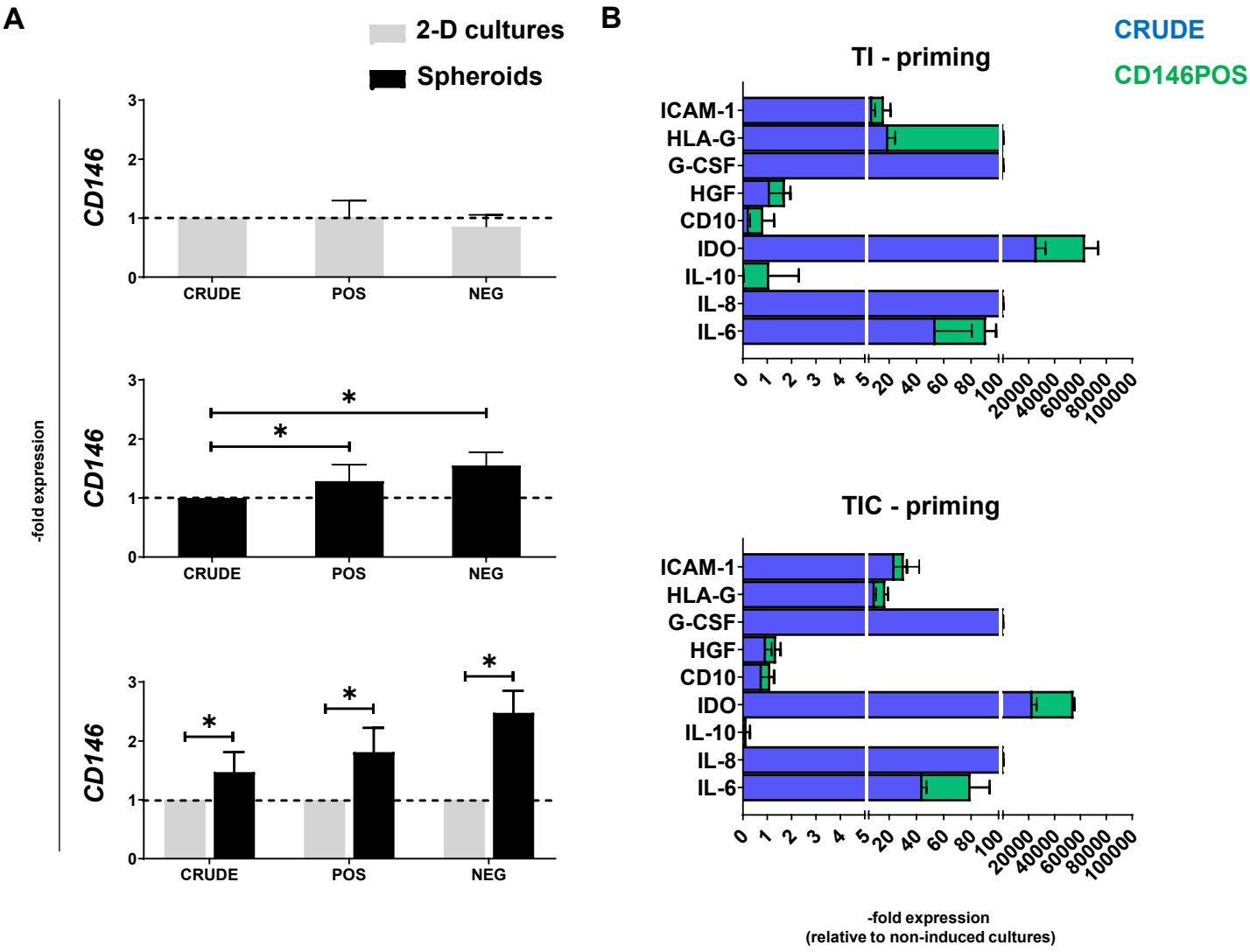

Supplementary Figure 2

A

Fractions	Significantly (p<0.05) UP-regulated post-TI stimulation	N	Significantly (p<0.05) DOWN-regulated post-TI stimulation	N
Crude	IFN-γ, IL-6, IL6 sR, IL-8, IP-10, MCP-2, M-CSF, MIP-1-α, MIP-1-β, RANTES, TNF-α, EGF R, NT-3, TGF-β2	**14**	Eotaxin-2 , G-CSF, GM-CSF, sTNF-RI, PDGF-BB, FGF-2, β-NGF, EGF, FGF-4, GDNF, HGF, IGFBP-1, M-CSF R	**13**
POS	ICAM-1, IFN-γ, IL-4, IL-6, IP-10, MCP-2, MIP-1-α, RANTES, TNF-α, AR, FGF-2, β-NGF, EGF, EGF R, GM-CSF, IGFBP-1, M-CSF R, NT-4, PDGFR-α, PDGF-AB, TGF-β1, TGF-β2, VEGF-A, VEGF R2, VEGF R3, VEGF D	**26**	SCF	**1**
NEG	ICAM-1, IFN-γ, IL-8, IP-10, MCP-2, MIP-1-α, RANTES, TNF-α, PIGF	**9**	IL-15, IL-16, TNF-β, sTNF-RI, β-NGF, FGF-4, IGFBP-1, IGFBP-3 VEGF R2	**9**

B

Fractions	Significantly (p<0.05) UP-regulated post-TIC stimulation	N	Significantly (p<0.05) DOWN-regulated post-TIC stimulation	N
Crude	ICAM-1, IFN-γ, IL-8, IL-12-p40 (IL-12-β), IL-12-p70 (IL-12-β), IL-15, IP-10, MCP-2, M-CSF, MIP-1-α, MIP-1-β, MIP-1-δ, RANTES, TNF-α, NT-3, TGF-α, TGF-β1, TGF-β2	**18**	sTNF-RI, PDGF-BB, FGF-2, EGF, FGF-4, IGF-I, IGF-I sR, PDGF-AA, PDGF-AB, PIGF, SCF	**11**
POS	ICAM-1, IFN-γ, IP-10, MCP-2, MIP-1-α, RANTES, TNF-α, AR, FGF-2, EGF, FGF-6, IGFBP-1, IGF-I, PDGFR-α, PDGFR-β, PDGF-AA, PDGF-AB, PIGF, SCF R, TGF-β2, TGF-β3, VEGF-A, VEGF R2, VEGF R3	**24**	Eotaxin-2	**1**
NEG	G-CSF, IL-3, IL-16, IGFBP-1, IGFBP-3	**5**	ICAM-1, IFN-γ, IL-8, IL-12-p70 (IL-12-β), IP-10, MCP-2, MIP-1-α, MIP-1-δ, RANTES, TNF-α, sTNF-RII, HB-EGF	**12**

Supplementary Figure 3

A

UP-regulated TI-induced IFP-MSC

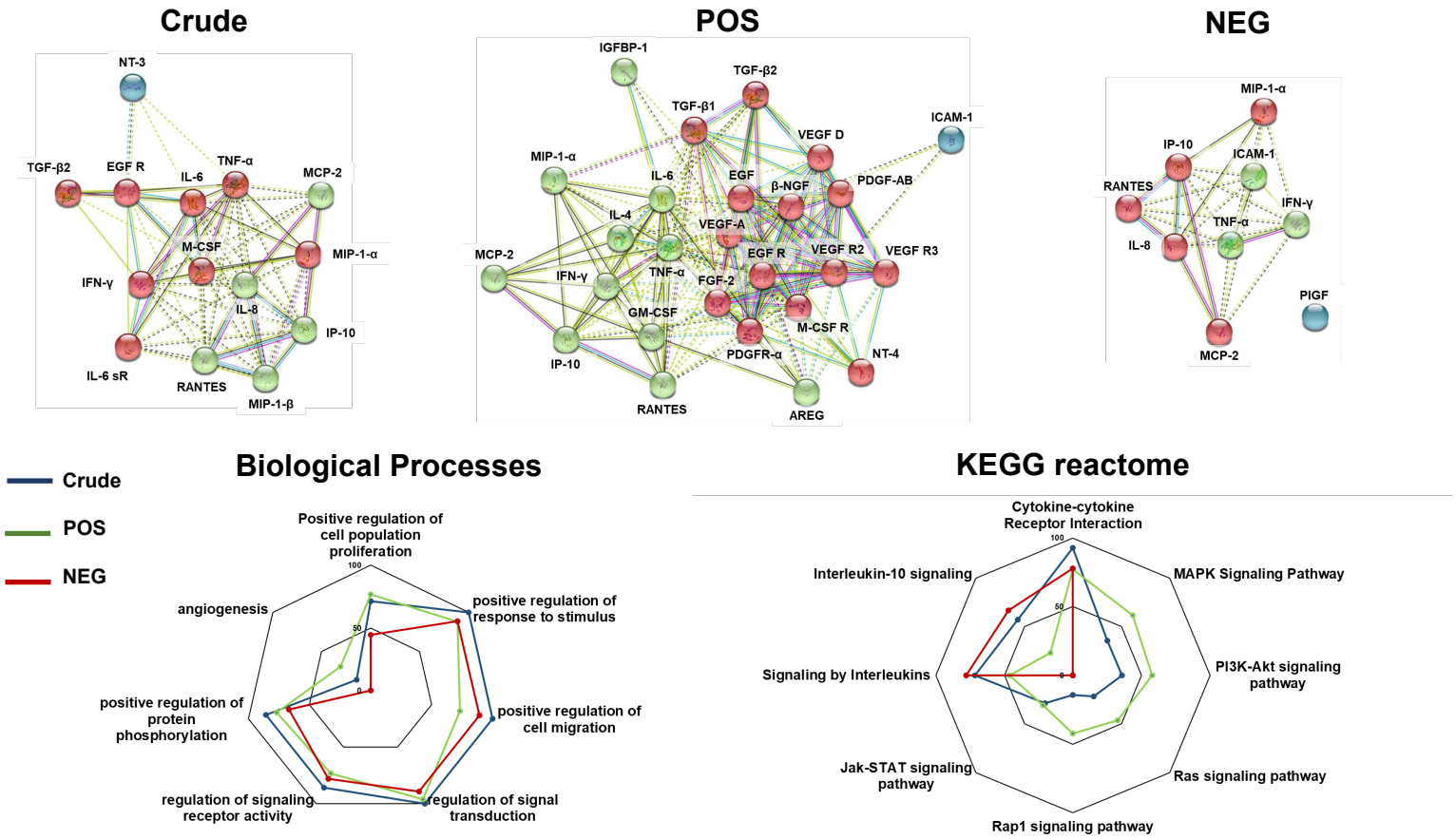

B

UP-regulated TIC-induced IFP-MSC

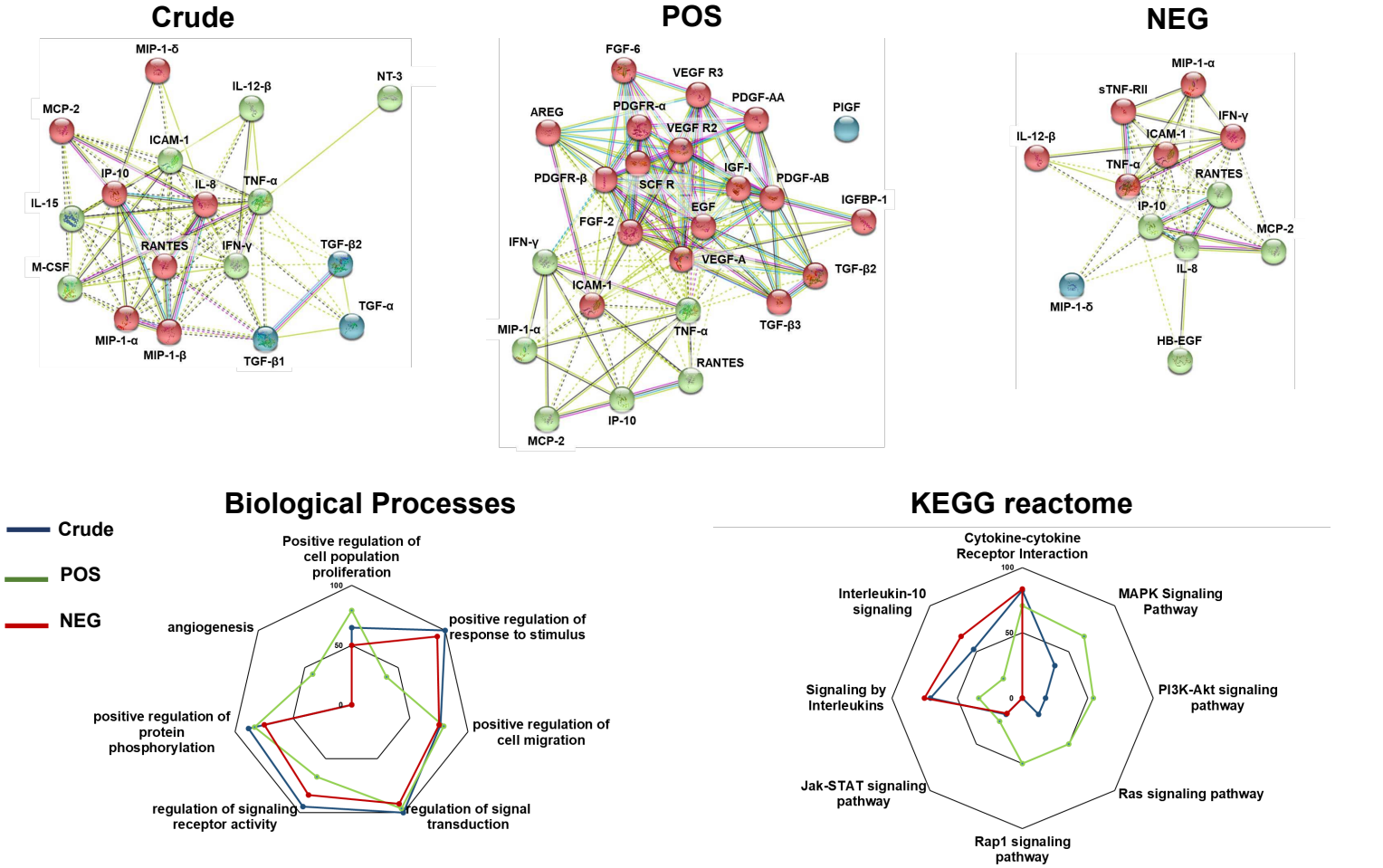

Supplementary Table S1. Transcripts and primers.

TRANSCRIPT NAME	PRIMERS
BGLAP	Forward: *CAG CGA GGT AGT GAA GAG AC* Reverse: *TGA AAG CCG ATG TGG TCA G*
OMD	Forward: *ACG ATG ATC CTG ACA ATG CTC* Reverse: *GTA TAG GTT TTG TGA AGT CGT AAG TG*
FABP4	Forward: *AAG AAG TAG GAG TGG GCT TTG* Reverse: *TCA ACG TCC CTT GGC TTA TG*
PPARγ	Forward: *GCC TGC ATC TCC ACC TTA TT* Reverse: *AGC GGG AAG GAC TTT ATG TAT G*
ACAN	Forward: *TGT GGG ACT GAA GTT CTT GG* Reverse: *AGC GAG TTG TCA TGG TCT G*
COMP	Forward: *GAC AGT GAT GGC GAT GGT ATA G* Reverse: *TCA CAA GCA TCT CCC ACA AA*
IL-6	Forward: *GTA GCC GCC CCA CAC AGA CAG CC* Reverse: *GCC ATC TTT GGA AGG TTC*
IL-8	Forward: *GAA CTG AGA GTG ATT GAG AGT* Reverse: *CTT CTC CAC AAC CCT CTG*
CD10	Forward: *CTG TGG GAT GAG GAG GTT AAA G* Reverse: *GGA GGC TAA AGC AGG AGA ATA G*
ICAM-1	Forward: *AGG AGG TGG TAA GAG AGA AGA G* Reverse: *TAA GGG TGG GAG GAG GAT TT*
G-CSF	Forward: *AGC TTC CTG CTC AAG TGC* Reverse: *TTC TTC CAT CTG CTG CCA GAT GGT*
HGF	Forward: *ATG TGG GTG ACC AAA CTC CTG* Reverse: *CTA TTG AAG GGG AAC CAG AGG*
IL-10	Forward: *GCC TAA CAT GCT TCG AGA TC* Reverse: *TGA TGT CTG GGT CTT GGT TC*
HLA-G	Forward: *GCT GCT GTG CTG TGG AGA A* Reverse: *TCT GGA ACA GGA AAG GTG ATT GG*
IDO	Forward: *AGA GTC AAA TCC CTC AGT CC* Reverse: *AAA TCA GTG CCT CCA GTT CC*
GAPDH	Forward: *TAC GTC GTG GAG TCC ACT GG* Reverse: *GCC AAC GTG TCA GTG GTG GA*

Supplementary Table S2. Human mesenchymal stem cell qPCR array plate genes and their classification.

TRANSCRIPT NAME	CLASSIFICATION
PPARG, RHOA, CEBPA, CEBPB, LEPR	Adipogenic
HAT1, ITGAX, KAT2B, SOX9, ACAN, COL2A1, MMP13, CSPG4	Chondrogenic
BMP4, TGFB1, TGFB3, BMP6, KDR, MSX1, MSX2, BMP2, PRRX1	Chondrogenic / Osteogenic
TWIST2, ANPEP, CASP3, CD44, ENG, ERBB2, FUT4, FZD9, ITGA6, ITGAV, MCAM, NGFR, NT5E, PDGFRB, PROM1, THY1, VCAM1, BDNF, CD200, COL10A1, FGF18, DLX2, DLX5, PDGFRA	MSC
CTNNB1, EGF, HGF, ICAM1, IFNG, IGF1, IL10, IL1B, IL6, ITGB1, KITLG, MMP2, NES, NUDT6, PTPRC, SLC17A5, TNF, VEGFA, VIM, VWF, JAG1, NOTCH1, GDF15, SMAD4, HIC1	MSC-related/Angiogenesis
ALPL, IBSP, SP7, BGLAP, BMP7, COL1A1, FGF10, HDAC1, PTK2, SMURF1, SMURF2, TBX5, RUNX2, FGF9	Osteogenic
FGF2, LIF, SOX2, TERT, GDF5	Stemness
GAPDH, RN18S1, ACTB, TBP, UBC Positive Control	Housekeeping / Control

Figures

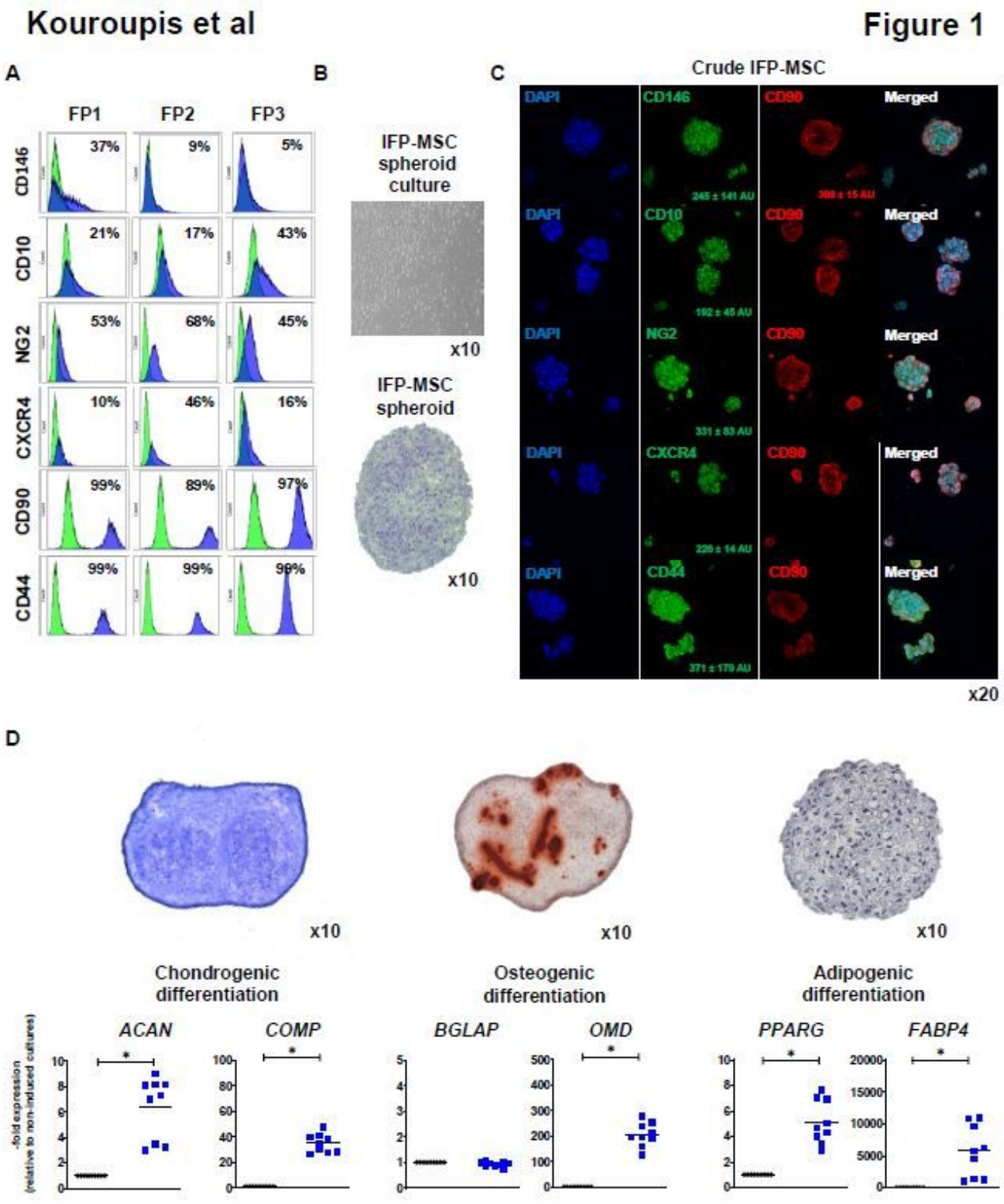

Figure 1

IFP-MSC spheroid immunophenotypic profile and tripotentiality. (A) In 2D settings, Crude IFP-MSC show stable MSC-related phenotypic profile with high expression levels for CD44 and CD90 markers and increased donor-to-donor variability in CD10, CD146, and CXCR4 expression levels. (B and C) Upon

seeding in gas-permeable culture plates, Crude IFP-MSC can generate multiple sized spheroids (100-300μm) with enhanced expression of CD90, CXCR4, CD10, and NG2. CD146 and CD44 show variable expression levels between spheroids. (D) IFP-MSC spheroids can efficiently differentiate towards chondrogenic, osteogenic and adipogenic lineages after specific induction in gas-permeable plates. Quantitative molecular profiling showed that differentiation-related markers in induced IFP-MSC spheroids were increased compared to non-induced cultures, indicating their mature status. All experiments (n=3) were performed independently and data are presented as mean ± SD (*p<0.05).

Kouroupis et al **Figure 2**

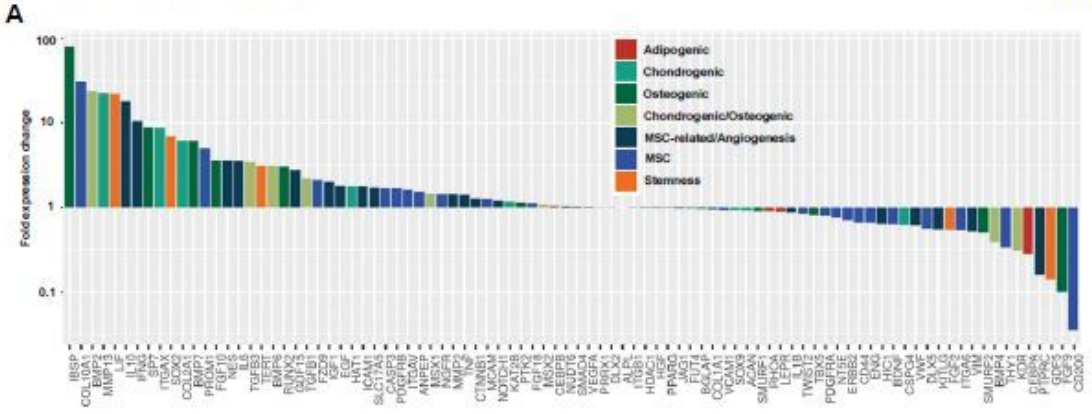

Classification	Genes	Median Fold Change (3D spheroids to 2D cultures)	P-Value
Stemness	LIF, SOX2, TERT, FGF2, GDF5	2.69735	0.4137
Chondrogenic	MMP13, ITGAX, COL2A1, HAT1, KAT2B, SOX9, ACAN, CSPG4	1.69247	0.55794
MSC-related/ Angiogenesis	IL10, IFNG, NES, IL6, GDF15, IGF1, EGF, ICAM1, SLC17A5, MMP2, TNF, CTNNB1, NOTCH1, NUDT6, SMAD4, VEGFA, ITGB1, HGF, JAG1, IL1B, HIC1, VWF, KITLG, VIM, PTPRC	1.28867	0.28437
Chondrogenic / Osteogenic	BMP2, TGFB3, BMP6, TGFB1, MSX1, MSX2, PRRX1, BMP4, KDR	1.26607	0.91703
Osteogenic	IBSP, SP7, BMP7, FGF10, RUNX2, PTK2, ALPL, HDAC1, BGLAP, COL1A1, SMURF1, TBX5, SMURF2, FGF9	1.10396	0.03289
Adipogenic	CEBPB, PPARG, RHOA, LEPR, CEBPA	0.90238	0.36788
MSC	COL10A1, PROM1, FZD9, CASP3, PDGFRB, ITGAV, ANPEP, NGFR, MCAM, FGF18, DLX2, FUT4, VCAM1, TWIST2, PDGFRA, NT5E, ERBB2, CD44, ENG, BDNF, DLX5, ITGA6, THY1, CD200	0.86973	0.28865

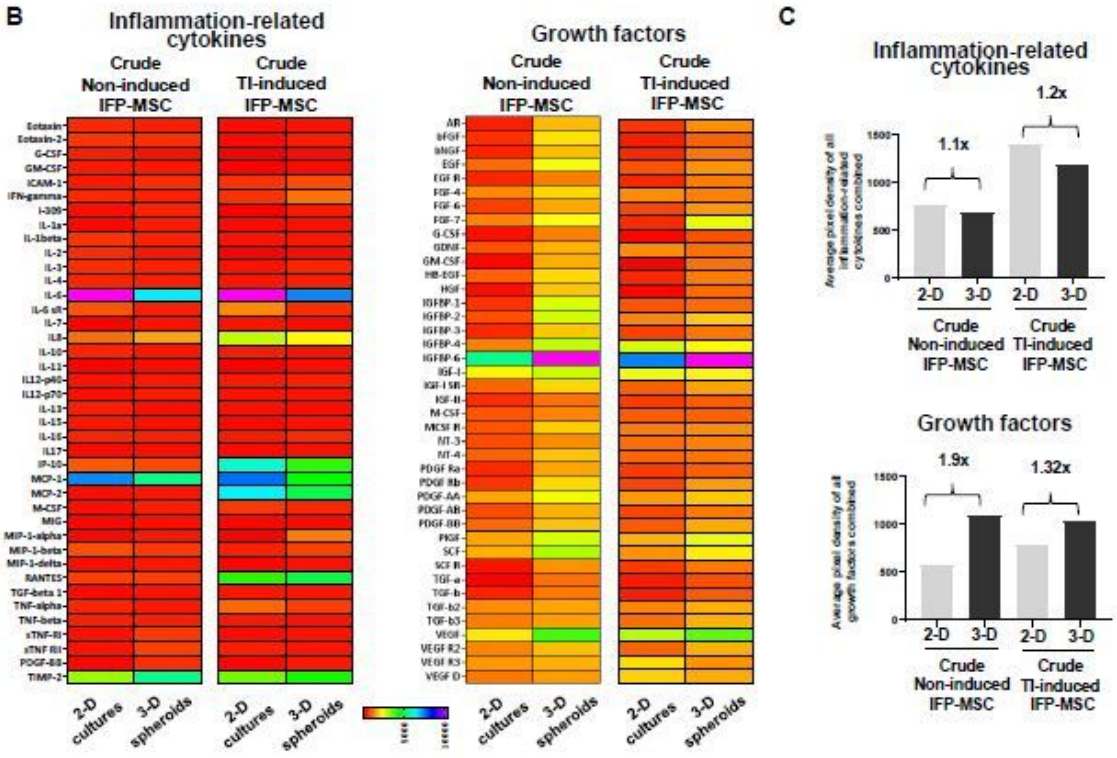

Figure 2

Molecular and secretory profiling of 2-D IFP-MSC and IFP-MSC spheroids. (A) Molecular profiling of non-induced IFP-MSC spheroids versus non-induced 2-D IFP-MSC cultures revealed that 49 out of 90 genes tested were higher expressed in IFP-MSC spheroids with 24 genes being more than two-fold higher. Genes tested were grouped in phenotype/function-related cohorts. (B and C) The secretory profile of inflammation-related cytokines revealed that non-induced IFP-MSC spheroids show significantly ($p<0.05$) higher secretion of 13 and lower secretion of 5 (IL-6, IL-6sR, IL-16, MIP-1-β, TNF-α) out of 40 secreted proteins tested compared to naïve 2-D IFP-MSC cultures. In addition, non-induced IFP-MSC spheroids show significantly ($p<0.05$) higher secretion of 36 out of 41 secreted protein tested. Heat maps colours are assigned according to a molecule concentration relative scale, from 0 to 10,000. All experiments were performed independently (n=2).

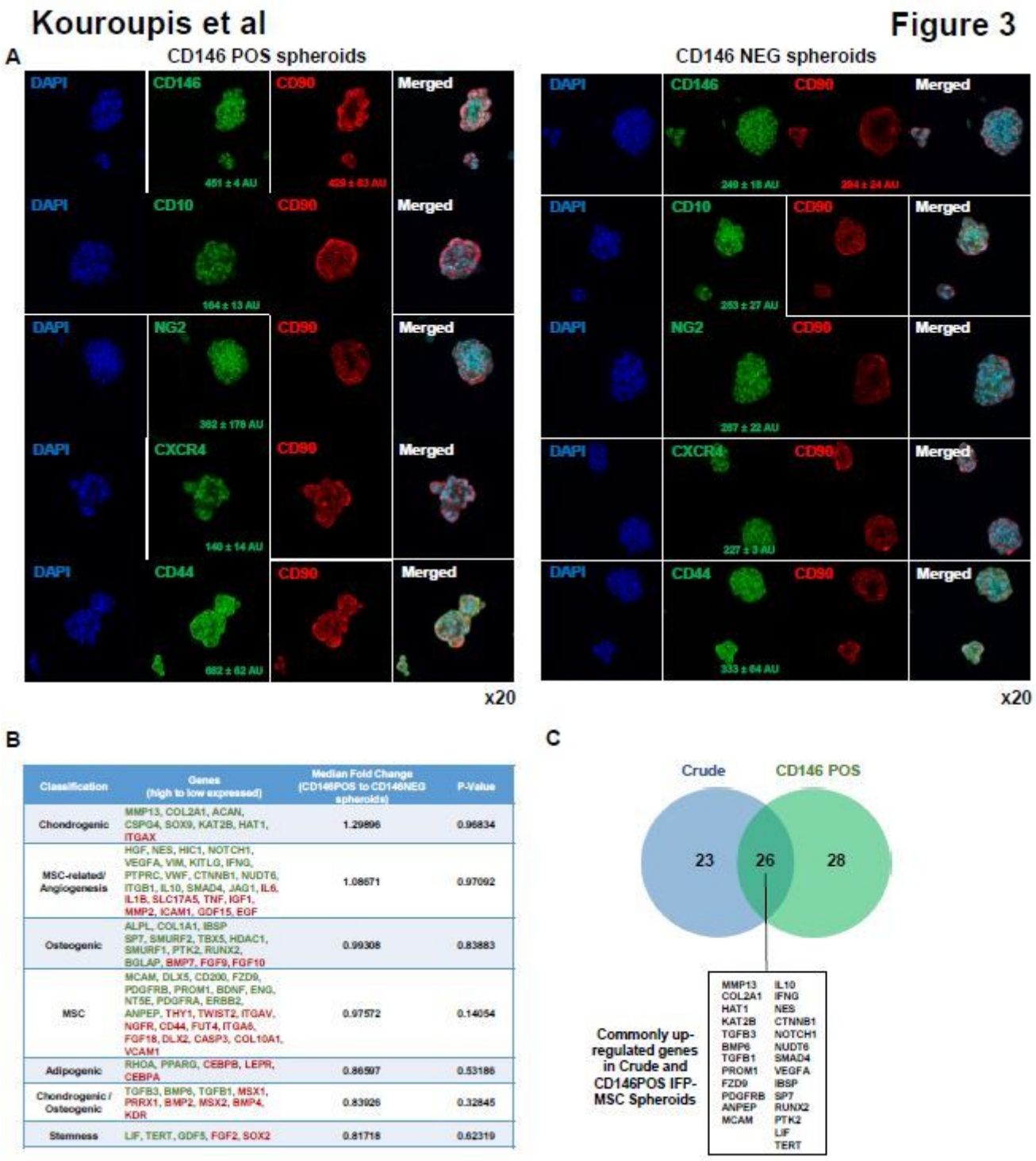

Classification	Genes (high to low expressed)	Median Fold Change (CD146POS to CD146NEG spheroids)	P-Value
Chondrogenic	MMP13, COL2A1, ACAN, CSPG4, SOX9, KAT2B, HAT1, ITGAX	1.29896	0.96834
MSC-related/ Angiogenesis	HGF, NES, HIC1, NOTCH1, VEGFA, VIM, KITLG, IFNG, PTPRC, VWF, CTNNB1, NUDT6, ITGB1, IL10, SMAD4, JAG1, IL6, IL1B, SLC17A5, TNF, IGF1, MMP2, ICAM1, GDF15, EGF	1.08671	0.97092
Osteogenic	ALPL, COL1A1, IBSP SP7, SMURF2, TBX5, HDAC1, SMURF1, PTK2, RUNX2, BGLAP, BMP7, FGF9, FGF10	0.99308	0.83883
MSC	MCAM, DLX5, CD200, FZD9, PDGFRB, PROM1, BDNF, ENG, NT5E, PDGFRA, ERBB2, ANPEP, THY1, TWIST2, ITGAV, NGFR, CD44, FUT4, ITGA6, FGF18, DLX2, CASP3, COL10A1, VCAM1	0.97572	0.14054
Adipogenic	RHOA, PPARG, CEBPB, LEPR, CEBPA	0.86507	0.53186
Chondrogenic / Osteogenic	TGFB3, BMP6, TGFB1, MSX1, PRRX1, BMP2, MSX2, BMP4, KDR	0.83926	0.32845
Stemness	LIF, TERT, GDF5, FGF2, SOX2	0.81718	0.62319

Figure 3

Immunophenotype and molecular profile of CD146-selected IFP-MSC spheroids. (A) Upon seeding in gas-permeable culture plates, CD146POS IFP-MSC spheroids show as expected higher expression levels of CD146 (451±4 AU vs 241±18 AU) and higher expression levels of NG2 (362±178 AU vs 287±22 AU), whereas CD146NEG IFP-MSC spheroids show higher expression levels of CD10 (253±27 AU vs 164±13 AU) and CXCR4 (227±3 AU vs 140±14 AU). (B) Molecular profiling of CD146POS versus CD146NEG IFP-

MSC spheroids revealed that 55 out of 90 genes tested were higher expressed in CD146POS IFP-MSC spheroids with IFP-MSC spheroids reverse synovitis/IFP fibrosis 12 genes being more than two-fold higher (MCAM, HGF, ALPL, DLX5, NES, MMP13, CD200, COL1A1, FZD9, PDGFRB, HIC1). Genes tested were grouped in phenotype/function-related cohorts. (C) 26 genes are shared between Crude and CD146POS spheroids, indicating similarities in their molecular signatures. However, upon TI- or TIC-induction most of the immunoregulatory-related genes tested show up-regulated expression levels in CD146POS spheroids. All experiments were performed independently (n=3).

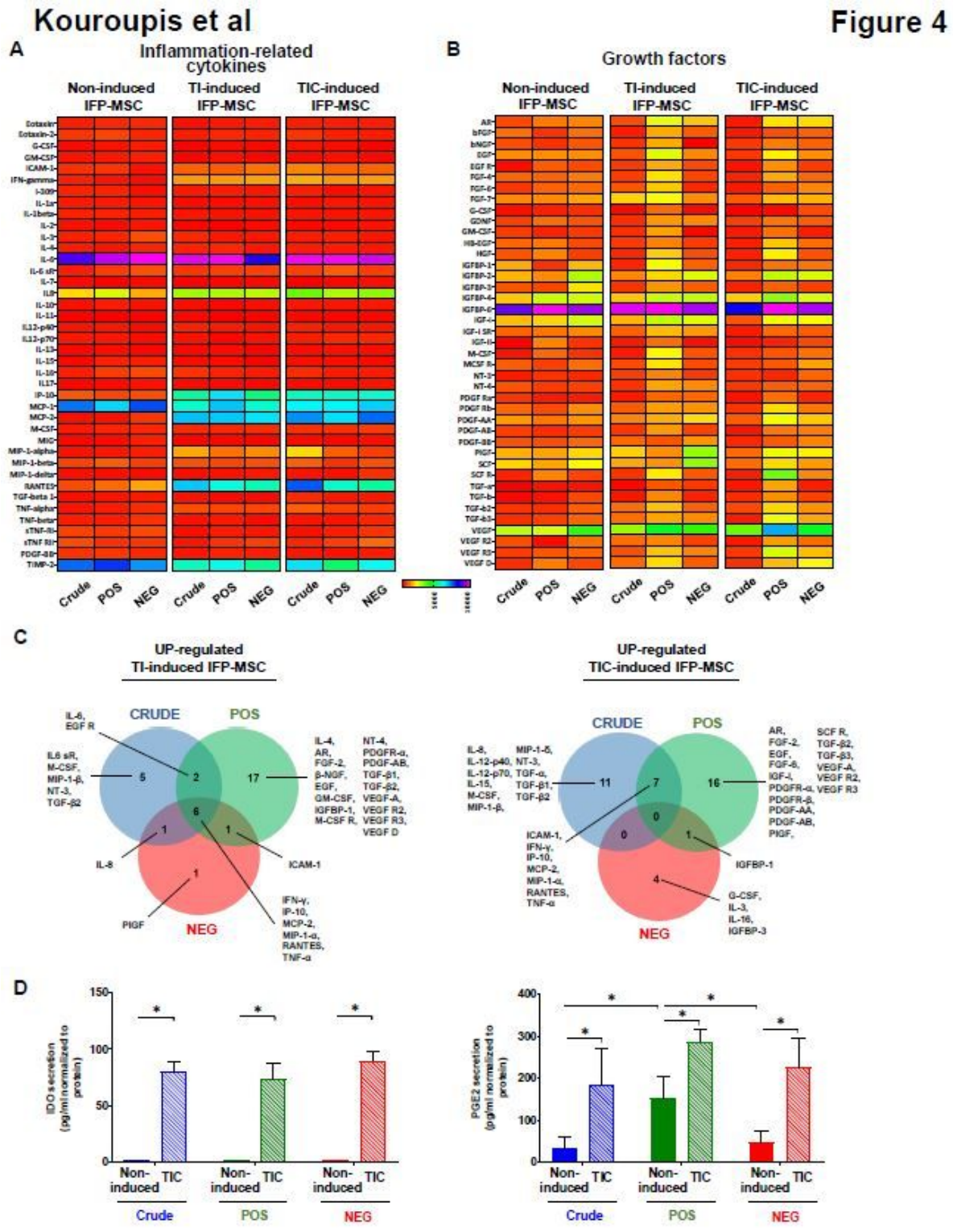

Figure 4

Secretory profiling of Crude and CD146-selected IFP-MSC spheroids with and without exposure to inflammatory/fibrotic cues. (A and B) Crude and CD146-selected IFP-MSC spheroids show similar inflammation-related secretory profiles both in non-induced and TI- or TIC-induced conditions. However, their secretory profiles of reparative growth factors were distinct and characterized by the secretion of different numbers and types of proteins. Heat maps colours are assigned according to a molecule concentration relative scale, from 0 to 10,000 (n=2). (C) In both TI- and TIC-induced conditions, CD146POS IFP-MSC spheroids show higher number of secreted proteins. Among the proteins with up-regulated secretion levels 6 and none proteins are commonly shared between the three different cohorts (crude, CD146POS, CD146NEG) after TI and TIC induction, respectively. Venn diagram showing shared proteins amongst the three different cohorts (Crude, CD146POS, CD146NEG) after TI and TIC induction. All experiments were performed independently (n=2). (D) In non-induced cohorts IDO secretion is almost absent whereas PGE2 secretion is evident in all three cohorts. TIC induction result in increased IDO and PGE2 secretion levels (*$p<0.05$, n=3).

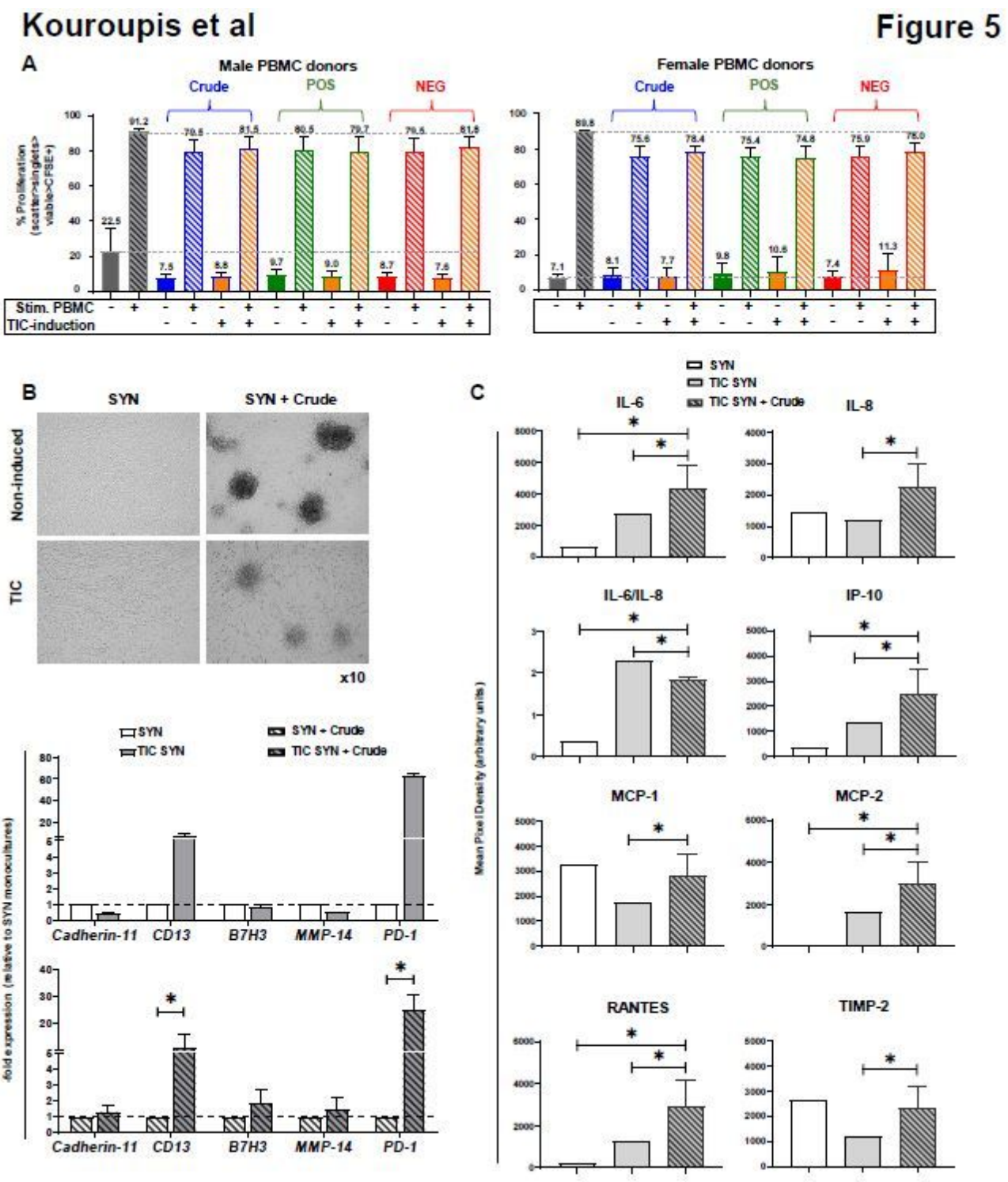

Figure 5

Immunomodulatory functionality of Crude IFP-MSC spheroids. () CFSE-labeled, PMA/IO-activated human PBMC showed a proliferation of ~91.2% for male PBMC donors and of ~89.9% for female PBMC donors, which was suppressed in a PBMC gender-dependent manner by co-culture with non-induced Crude or CD146-selected IFP-MSC spheroids (*p<0.05, n=3). (B) In both non-induced and TIC-induced SYN, non-induced Crude IFP-MSC spheroids can effectively form explant-cultures on synoviocyte monolayer

whereas TIC induction of SYN significantly (*p<0.05) up-regulate inflammatory genes such as CD13 and PD-1. (C) SYN/IFP-MSC spheroid co-cultures resulted in significantly (*p<0.05) higher secretion of immunomodulatory proteins (IL-6, IL-8, IP-10, MCP-1, MCP2, RANTES, TIMP-2) compared to TIC-induced SYN alone. All experiments were performed independently (n=3).

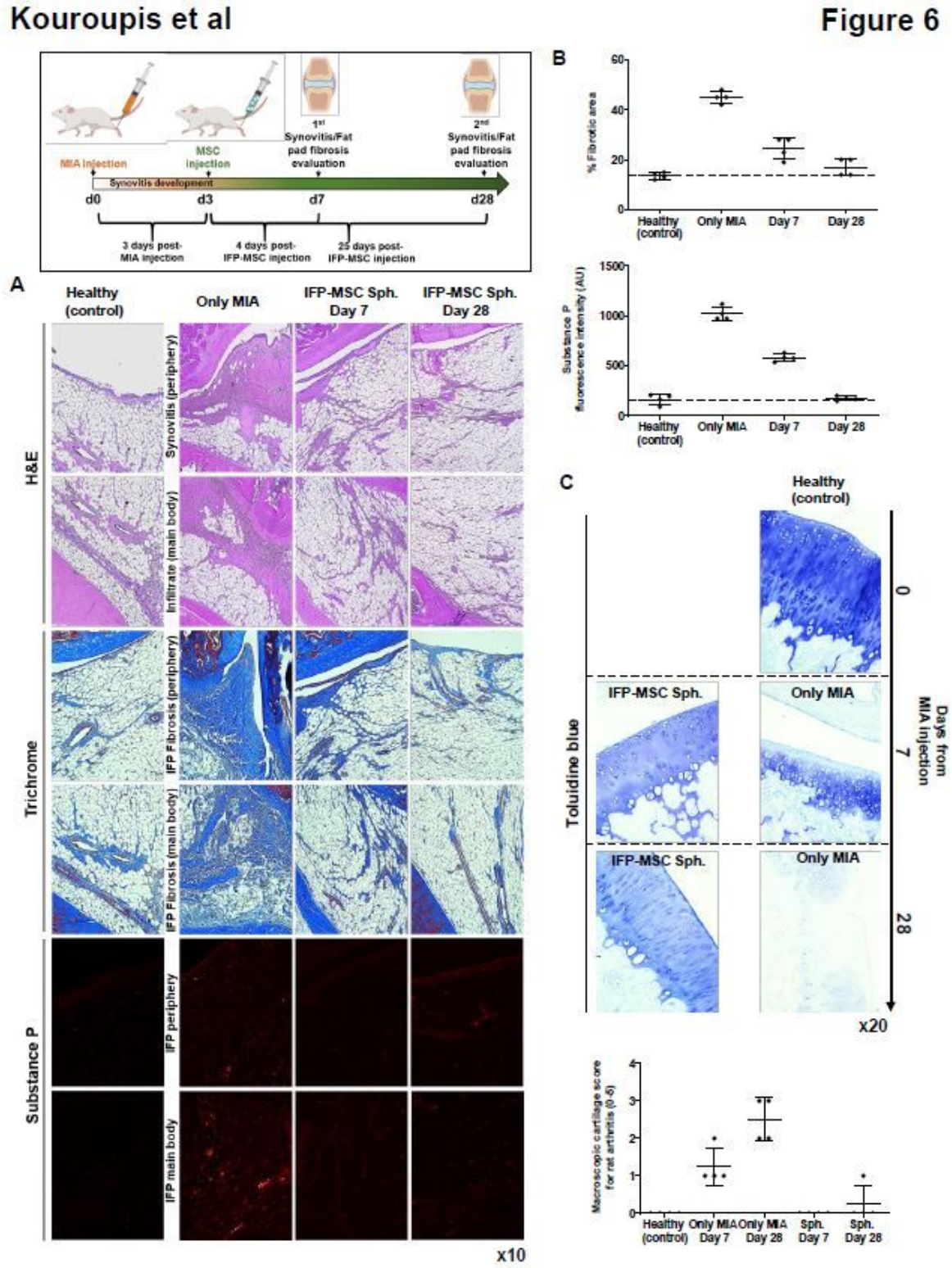

Figure 6

IFP-MSC spheroids effectively reverse synovitis and IFP fibrosis in vivo. Schematic indicating the generation of acute synovitis/IFP fibrosis rat model, therapeutic intervention and chronological evaluation. (A and B) Hematoxylin/Eosin staining (top 2 panels), Masson's trichrome staining (middle two panels) and Substance P immunolocalization (lower 2 panels) in sagitally-sectioned knees of representative rats for healthy control, injected only with MIA or with both MIA and IFP-MSC spheroids. Compared with only MIA injected IFP-MSC spheroids reverse synovitis/IFP fibrosis group, which showed a significant synovitis and IFP fibrosis with cellular infiltrates, a striking correlation was found between IFP-MSC spheroid treatment and the effect reducing inflammation and fibrosis after 3 and 25 days of a single intra-articular IFP-MSC injection. (C) After MIA injection, all animals developed OA changes that resulted in OA lesions on day 28. IFP-MSC spheroid injection group didn't show any major OA lesion development whereas articular cartilage sGAG content was preserved which was evident by the strong toluidine blue staining.

Supplementary Files

This is a list of supplementary files associated with this preprint. Click to download.

- FigS1.JPG
- FigS2.JPG
- FigS3.JPG
- GraphicalAbstract.JPG
- TableS1.JPG
- TableS2.JPG